ADA072018

Spectroscopy and X-Radiation from Exploded-Wire Arrays and Gas Puff Plasmas

P. BURKHALTER

X-Ray Optics Branch
Radiation Technology Division

and

J. DAVIS

Plasma Radiation Group
Plasma Physics Division

March 16, 1979

79 03 23 04

NAVAL RESEARCH LABORATORY
Washington, D.C.

DDC
RECEIVED
AUG 2 1979
D

SECURITY CLASSIFICATION OF THIS PAGE (When Data Entered)

REPORT DOCUMENTATION PAGE		READ INSTRUCTIONS BEFORE COMPLETING FORM
1. REPORT NUMBER NRL Memorandum Report 3934	2. GOVT ACCESSION NO.	3. RECIPIENT'S CATALOG NUMBER
4. TITLE (and Subtitle) SPECTROSCOPY AND X-RADIATION FROM EXPLODED-WIRE ARRAYS AND GAS PUFF PLASMAS		5. TYPE OF REPORT & PERIOD COVERED Interim report on a continuing NRL problem.
		6. PERFORMING ORG. REPORT NUMBER
7. AUTHOR(s) P. Burkhalter and J. Davis		8. CONTRACT OR GRANT NUMBER(s)
9. PERFORMING ORGANIZATION NAME AND ADDRESS Naval Research Laboratory Washington, D.C. 20375		10. PROGRAM ELEMENT, PROJECT, TASK AREA & WORK UNIT NUMBERS NRL Problem H02-26K DNA Subtask T99QAXLB203
11. CONTROLLING OFFICE NAME AND ADDRESS		12. REPORT DATE March 16, 1979
		13. NUMBER OF PAGES 95
14. MONITORING AGENCY NAME & ADDRESS(If different from Controlling Office)		15. SECURITY CLASS. (of this report) UNCLASSIFIED
		15a. DECLASSIFICATION/DOWNGRADING SCHEDULE

16. DISTRIBUTION STATEMENT (of this Report)

Approved for public release; distribution unlimited.

17. DISTRIBUTION STATEMENT (of the abstract entered in Block 20, if different from Report)

19. KEY WORDS (Continue on reverse side if necessary and identify by block number)

Wire plasmas
Gas puffs
Spectroscopy

PI (Physics International)

20. ABSTRACT (Continue on reverse side if necessary and identify by block number)

In this report results are presented for three separate experiments involving multiple exploded wire arrays and puff gas plasmas. The first section deals with the analysis and interpretation of x-ray line spectra from a variety of exploded multiple wire arrays including Al, glass, Ti, SS, Mo, and W wires. The second section deals with x-ray spectra from puff gas experiments at PI for Ne, Ar, Kr, and Xe gases. Finally, we conclude with a discussion of x-ray spectra from a gas puff Z-pinch device, operated at the University of California, Irvine, that provides both spatial and spectral information of Ar x-ray emission.

DD FORM 1473 EDITION OF 1 NOV 65 IS OBSOLETE
1 JAN 73
S/N 0102-014-6601

i

SECURITY CLASSIFICATION OF THIS PAGE (When Data Entered)

CONTENTS

INTERPRETATION OF X-RAY LINE SPECTRA FROM EXPLODED-WIRE ARRAYS

X-RAY SPECTRA FROM GAS-PUFF EXPERIMENTS AT PI

X-RAY SPECTRA FROM A GAS-PUFF Z-PINCH DEVICE

FOREWORD

The understanding of exploding multiple wire and gas puff plasmas from x-ray observations depends on how well the plasma state can be described quantitatively during the emission process. The evolution of the plasma up to and during the radiation pulse is a complex problem involving competing physical processes and is currently under intensive investigation at NRL. Important understanding of the plasma can be gained from the diagnosis of the emitted radiation. Our approach to the problem here is to combine the results of the spectral observations with a simple plasma model that stresses the ionization and radiation dynamics of a multi-level atomic model. The size of the emitting region is estimated from x-ray pinhole data together with measurements of the intensity of diagnostically important spectral lines. The plasma model is then employed to calculate x-ray spectra for selected lines and continuum. These calculations yield reasonable estimates of the average plasma temperature and density which exist during the radiation pulse.

In this report we will confine our discussion to specific puff gas and multiple wire results. The report is structured in the following manner: the first part is concerned with the interpretation of x-ray line spectra from exploded-wire arrays, the second part discusses x-ray spectra from gas puff experiments at Physics International, and finally we conclude with a discussion of x-ray spectra from a gas puff Z-pinch device obtained from a series of experiments done at the University of California. The temperatures and densities were inferred from a plasma model discussed in an accompanying NRL Memorandum report.

iv

INTERPRETATION OF X-RAY LINE SPECTRA FROM
EXPLODED-WIRE ARRAYS*

I.   INTRODUCTION

X-ray spectra in the 1-7 keV region have been recorded with convex,
curved-crystal spectrographs in the PITHON and BLACKJACK 4 high voltage
exploded-wire generators. The spectra were recorded from the plasma
implosion formed at the center of the symmetrical imploded-wire arrays.
The x-ray data, collected throughout the periodic table (Mg thru W) on
No-Screen X-ray film, were processed to obtain relative spectral inten-
sities. Temperatures and densities were estimated for the entire implo-
sion region from line ratio techniques and the slopes of the continuum
in exploded-Al-wire spectra. The plasma models used were the coronal model
with dielectronic recombination, average atom model calculations, and a
collisionally-dominated, radiation transport code with a cylindrical
temperature input profile together with published plasma x-ray line ratio
data.

II. EXPERIMENTAL

Symmetrical-six-wire arrays were exploded in the PITHON at Physics
International Company (P.I.) (1) and the BLACKJACK 4 generator at
Maxwell Laboratories, Inc. X-ray spectra were collected, processed, and
interpreted from Al, glass, Ti, stainless steel, Mo, and W wires. The
x-ray film data selected were representative of spectral data from shots

---

* This section was co-authored with J. Rauch, W. Clark, G. Dahlbacka,
  and R. Schneider.

forming good plasma implosions as evidenced from intense x-ray signals
using active detectors. Pinhole images through 100 μm and 50 μm
apertures were available from two Al shots taken at Physics International.

Convex, curved crystal geometries were used on both generators,
mostly with two crystals recording simultaneous data onto No-Screen
x-ray film. At P. I., the crystals used were KAP (15.9 mm-radius,
2d = 26.6 Å) graphite, (2d = 6.7 Å) and LiF (12.6-mm radius) (2d = 4.03 Å)
and at Maxwell, KAP (31.8-mm radius) and LiF (6.3 mm radius) spectrographs
collected the x-ray spectra. Thin absorption filters of Kimfoil and
Kapton were used to record Al data and thicker mylar step filters allowed
data collection at various exposure levels on the same film. Valuable
high-dispersion Al spectra were recorded on a few of the shots from both
generators. The spectra were scanned at the Naval Research Laboratory
(N.R.L.) with a digitizing Grant scanning densitometer. Film densities
were recorded every 10 μm across the films using a 20 μm wide densitometer
slit width. This was adequate for profile resolution as the x-ray line
widths varied mostly in the range of 100-300 μm. The film densities were
converted to spectral intensities using No-Screen sensitometric data of
Dozier, et al. (2), x-ray absorption coefficients published by Henke (3)
for the filters, and unpublished, curved-crystal response data calculated
by Brown (4). In this report the spectral data are reported as relative
intensities of the x-ray emission incident on the x-ray crystals. X-ray
line ratios were obtained from the spectral peaks.

Temperature predictions were made in this work from various plasma
models. The recombining temperatures were determined from the dielectronic
satellites-to-resonance line ratios in Al and Si based on line ratios

-2-

published by Bhalla and Gabriel (5) and were estimated from the slopes of the free-bound H-like continuum in the Al spectra. Temperatures for the hot plasma emission were obtained from line ratios using coronal model calculations that include dielectronic recombination and a 1D multi-cell radiation model that incorporates a ray trace method to handle the radiation transport. The model assumes that the input energy from the generator dumps into a finite diameter (0.1 cm) implosion plasma formed at the center of the array with a constant ion density of 1×10^{19} ions/cm^3. A complete development and discussion of the multi-cell radiation transport model will be treated in a correlated report by Davis, et al. (6).

Density predictions were made from the ratio of the resonance-to-intercombination lines ($1s^2$-$1s2p$ ^{1}P/$1s^2$-$1s2p$ ^{3}P) in Al and Si using published calculations by Vinogradov, et al. (7) for laser-produced plasma densities. The merging of the high Rydberg transitions in Al and Ti allowed for density estimates. A density was determined for the Mo spectrum based on the average atom model calculations of Rozsnyai (8).

III. RESULTS

A. Al wire arrays

An Al spectrum from shot BL1 was collected on BLACKJACK 4 through 1/2-mil mylar step filters. Digitized spectral scans were made of five spectra and the spectral intensity trace for data collected through 1 1/2-mils of mylar is shown in Fig. 1. Al is readily stripped to the K-shell in exploded-wire plasmas. For this shot, the H-like resonance line (1s-2p) was about 60% the intensity of the He-like

resonance line ($1s^2$-$1s2p$ ^1P). These two lines are optically thick in a uniform hot, dense plasma of 10^{20} el/cm^3. The resonance lines require large correction for the absorption by the mylar filter. For these reasons, temperatures were determined also from the ratio of the H-like $1s$-$3p$ line and the He-like $1s^2$-$1s5p$ line. These lines are seen to be close in wavelength (near 6 Å) and are generally closer in exposure levels than are the resonance lines to the $2p$ level. Therefore uncertainties in data processing would be minimized (less than 5 percent) for the ratio of $1s$-$3p$ to $1s^2$-$1s5p$ lines. The $1s$-$3p$ line can be optically thin in Al. An agreement in temperature estimated from the two sets of line ratios provides reassurance of the consistency of the data processing and model predictions. A uniformly decreasing free-to-bound H-like continuum is seen between 6 and 4 Å in the spectrum. A plasma temperature of 550 eV is obtained for this spectrum. Line ratios and temperature estimates from various models are listed in Table I. The density value of 1 x 10^{20} el/cm^3 was obtained from the ratio of the He-like resonance-to-intercombination line. The higher Rydberg transitions in H-like $1s$-$4p$ to the $1s$-$9p$ lines were observed in the high dispersion spectrum for shot BL1.

The spectral intensities for the Al shot PI1 from PITHON are shown in Fig. 2 both in first and high dispersion. The entire H- and He-like spectra were recorded in the first order spectrum. The density from the $^1P/^3P$ ratio was 7 x 10^{19} el/cm^3. The higher Rydberg transitions were obtained with high dispersion from the (013) plane in KAP. The resolution achieved is comparable to that obtainable with a PET crystal ($2d = 8.726$ Å). In both the He-like and H-like series, transitions to the $9p$ level are the

-4-

last distinct high Rydberg transition. A density estimate of 3×10^{20} el/cm^3 is obtained from the series merging technique (9). The H-like 1s-3p and He-like 1s^2-1s5p lines were distinct in the high dispersion spectrum and a temperature value of 750 eV was obtained as a thin temperature estimate. This is the same as was obtained from the 1s-3p/1s^2-1s5p ratio in the Maxwell shot. A sequence of Al shots was taken on PITHON on six wire arrays with increasing input power. The spectral results are seen in Fig. 3. The first order spectrum for shot PI2 recorded the entire set of spectral lines. The density was determined to be 1×10^{20} el/cm^3 from the $^1P/^3P$ ratio. This shot formed a cooler implosion than PI1. In shot PI3 the He-like 1s^2-1s2p resonance lines were not recorded and in shot PI4 both the H-like and He-like resonance lines were missing. This cut off of the longer wavelength lines can be caused by a slight rotation of the spectrograph relative to the sources. In this series of shots the absence of the second-order spectra is caused by a spectrograph rotation. A somewhat larger entrance aperture for the KAP spectrograph would be beneficial in lessening the chances of spectral cutoff. The higher Rydberg transitions were fully recorded in these spectra and the ratio of the 1s-3p/1s^2-1s5p lines gave an indicated doubling of plasma temperature in the series. As the plasma temperature increased, the magnitude of the H-like free-bound continuum is seen to be enhanced relative to the spectral lines. Also, one can infer from the shape of the free-bound continuum in shot PI4 that the peak energy of the free electrons has increased.

A shot PI5 from a 12-wire array produced an Al spectrum similar to shot PI3. The slight differences in spectral line ratios and continuum slopes for shots PI5 and PI3 are reflected in the temperature estimates in Table I. Pinhole images of the plasma implosion were recorded through a 100 μm aperture on Kodak type AA film on shot PI5. The first film recorded the x-ray emission mainly above 1 keV. An over-exposure occurred on the first film; however, a second film recorded a readable image with the first film serving as a transmission filter. The pinhole image for x-ray continuum radiation above 3 keV was recorded in the pinhole image shown in the upper portion of Fig. 4. Two-dimension density contours of the pinhole image at two magnifications are shown. The contour step was set at 0.2 density units. Most striking are the intense regions of x-ray emission along the implosion. All the spectra in this report were collected without spatial resolution. It is probable that in the case of Al the recorded spectra were emitted from a few localized regions of about 500 μm in size, with cores of ≤ 100 μm. Unfortunately pinhole images were not available for the other Al spectra shown in this report except for shot PI2 shown in Fig. 5. The emission from this image also appears to be localized into small spots. Some of the more intense regions appeared split into several spots instead of localized spherical shapes seen in shot PI5.

B. Glass Wire Array

A six-wire array of glass fibers was exploded in PITHON yielding an x-ray spectrum of Si shown in Fig. 6. Superimposed on the spectrum were Al lines. The origin of the Al ions is presumed to arise from the Al anode. The cathode housing was brass in this experiment and aluminum

is not commonly found in glass at the percent level. The temperature determined from the ratio of the Si XIV (1s-2p)/Si XIII($1s^2$-1s2p) lines is 650 eV based on the coronal model. The same line ratio for the Al lines in this plasma yield the same 650 eV (thin) temperature based on the transport model calculations for an electron density of $\sim 10^{20}$ cm^{-3}. This is the density determined from the $^1P/^3P$ ratio in Si XIII. The free-bound continuum was too low for a recombination temperature determination in the Si spectrum. The glass shot PI6 was fired at about the same mass loading and input power as the Al shot PI1 which yielded a higher Al plasma temperature.

A second-order Si spectrum was recorded with the KAP crystal on this glass shot PI6. The well-dispersed Si XIII resonance lines are shown in Fig. 7. The $^1P/^3P$ ratio in He-like Si XIII gave the same 1×10^{20} el/cm^3 density estimate as was determined from the first-order spectrum. Analysis of the line intensities for the dielectronic recombination lines j and k gave a cool recombining plasma temperature estimate of 4.5×10^6 K or about 400 eV.

C. Ti Wire Arrays

The Ti spectra collected with LiF crystals for BLACKJACK (shot BL2) and PITHON (shot PI7) are shown together in Fig. 8. The He-like lines are the most dominant in each spectrum. The experimental intensity ratio for the H-like (1s-2p)/ He-like ($1s^2$-1s2p^{1}P) lines is ~ 3.5 in each spectrum. The temperature estimates for the Ti spectra are 2.0 keV with a coronal model that includes dielectronic recombination and 2.1 keV for the multi-cell transport model. For an assumed plasma ion density

-7-

of 10^{19} cm^{-3}, the 4.7 keV radiation for the Ti lines is optically thin

so that the temperature determinations are not opacity affected. The

density of the exploded-Ti-wire plasmas could not be determined from the

ratio of He-like ^{1}P/^{3}P because this ratio is density sensitive only above

10^{22} el/cm^{-3}. However a density estimate of 6×10^{20} el/cm^{-3} was obtained

from the series limit from the observation of the $1s^2$-1s7p line being the

last distinct line before series merging in shot BL2. The difference

in the spectra in regard to plasma temperatures was the evidence of Ne-

like lines seen in the PITHON shot indicating cool plasma formation

(temperature < 150 eV) that was not seen in the BLACKJACK 4 shot BL2.

D. Stainless Steel Array

The spectrum collected with the LiF crystal for shot BL3 from

BLACKJACK 4 is shown in Fig. 9. The most abundant ionization stage is

Li-like in both the Cr and Fe spectrum. The H-like Fe XXVI line is just

visible at ~ 1.8 Å. The Fe radiation is optically thin in exploded-wire

plasmas. A coronal temperature estimate of 1.5 keV is obtained for the

Fe spectrum. There is also evidence (Fe XIV-XVII lines) for cool plasma

formation with a coronal temperature of 150 eV.

The long wavelength stainless steel spectrum collected with the KAP

crystal is shown in Fig. 10. The most distinct Fe lines belong to

Li-like Fe XXIV and are identified in the figure together with lines from

Li-like Cr XXII. An Al spectrum was recorded in this shot. Al ions

could be introduced into the plasma from either the anode or cathode in

the BLACKJACK 4 generator. The plasma temperature determined from the

Al line ratio for the 1s-2p/$1s^2$-1s2p was 0.80 keV.

E. Mo Wire Array

The first-order KAP spectrum of an exploded-Mo-wire array shot PI8 in PITHON is shown in Fig. 11. The most intense and distinct lines in the spectrum arise from Ne-like Mo XXXIII. The position of the lines in Mo XXXIII and in F-like Mo XXXIV are indicated below the spectrum. The height of the line positions indicate the theoretical oscillator strengths. A detailed spectroscopic analysis of the complex exploded-Mo-wire spectra from both single and multi-wires has been recently completed (10). The region of the spectrum between 5.0 and 5.5 Å contain Na-like 2p-3s satellite lines as shown in Fig. 12. An analysis of the satellite-to-resonance line ratio predicts a temperature range of 2.5-3 keV, based on coronal calculations at low plasma densities (11). The ratio of the F-like to Ne-like spectral patterns indicate a coronal temperature of about 4 keV for the exploded-Mo-spectrum. Transitions to high Rydberg levels in Mo were examined in the spectrum recorded with a graphite crystal. Distinct lines to the 7p level were observed in Mo XXXIII. An electron density estimate of 10^{20} el/cm^3 was obtained using line broadening theory incorporated in the average atom model (12).

F. W Wire Arrays

W spectra were not obtained with the KAP spectrographs from either generator and therefore a temperature for the W thermal plasma could not be determined. The W thermal spectrum for single wires exploded in Gamble II were stripped into the M shell and intense 3d-4f lines in W^{+46} were observed (13). W spectra collected with LiF crystals in both generators were similar to that reported for single-W-wires (13). The spectra were the inner L-shell spectra of W produced by energetic electrons.

-9-

IV. SUMMARY AND DISCUSSION

The plasma temperatures and density determined from the interpretation of the exploded-wire arrays are summarized in Table II for wires Al through Mo. The most abundant ionization stage changes systematically from either He or H in Al to Ne-like in Mo. The temperatures for the higher power shots were roughly 0.5-0.85 keV for Al, 1.5-2 keV for Ti, Cr, Fe and 2.5-4 keV for Mo. Hotter plasma temperatures are therefore associated with the implosions from higher Z elements. It is not clear why the temperature determined from the Al and Fe spectral lines are different for ions in the same implosion (SS shot BL3); however, the origin of the ions in the plasma were different. In addition to the hot plasma temperatures, evidence of cooler plasma $\sim$ 150 eV was found in several spectra.

Much of the effort both experimentally and theoretically involved Al wire spectra in this work. The experimental line ratios for the two sets of H-like/He-like lines for Al spectra from the various P.I. and Maxwell Laboratory shots together with temperatures are given in Table I. The uncertainties in spectral line intensities and line ratios are estimated to be $\pm$ 20%. This is the level of agreement for the $1s$-$3p/1s^2$-$1s5p$ lines between the first and high dispersion spectrum in PITHON shot PI1 for this line ratio in Al spectra collected through different mylar step filters for the BLACKJACK 4 shot BL1. Factors contributing to uncertainties in spectral line intensities include variations in the diffraction responses for the curved KAP crystals and exposure irregularities due to grain size structure using No-Screen x-ray film. Differences in obtaining line ratios from peak heights or from integrating

-10-

line intensities were less than 10% for the KAP data. This agreement results because the line profiles are constant in the low dispersion found in the KAP spectral data for Al. Temperatures can be compared between those determined from the two sets of line ratios. For the PITHON shot PI1 and the BLACKJACK 4 shot BL1 the agreement between sets is within 15% for the thick and thin calculations, but agreement was not found for the PITHON shot PI2. For the three shots in which the $1s-2p/1s^2-1s2p$ ratios were available, the coronal temperature estimate is about midway between the thick and thin temperatures. If the x-ray spectral emission recorded for Al plasmas arises from a uniform plasma volume at 10^{20} el/cm^3 for a 0.1 cm diameter, then the actual Al plasma would have a temperature corresponding to the thick case. If the emission in the Al plasma is recorded predominately from intense emitting regions only 500 μm in size as suggested by the pinhole image contours, then the temperatures estimated for thin plasma would be appropriate. A better understanding of the origin of the Al spectral emission in plasma implosions requires spatial spectral data correlated with pinhole images. The temperatures obtained from the slopes of free-bound hydrogenic continuum are close to the values the transport model predicts for thick plasma cases. The two methods used for density determinations in Al plasmas have yielded results between 7×10^{19} to 3×10^{20} el/cm^3 for some average value of density corresponding to intense emitting regions of the plasma implosion. An electron density of $\sim 1 \times 10^{20}$ el/cm^3 is consistent with densities found in the higher Z-wire implosions and is lower than the 10^{21} el/cm^3 densities for single exploded-Al-wire plasmas determined by the same spectral techniques. If the density for the Al

-11-

implosion were an order of magnitude higher at 10^{21} el cm^3, the temperature determination from the ratio of the 1s-2p resonance lines would be lowered to 475 eV and the plasma would be thick even for 500 μm spots. The 1s^2-1s5p line is affected by opacity to a greater degree than the 1s-3p line and the temperatures determined by the two sets of line ratios would have a greater disagreement than found in Table I. The temperature determined by the line ratio 1s-3p/1s^2-1s5p would become 350 eV at densities of 10^{21} el/cm^3. The consistency of the plasma temperature and density determinations from within each spectrum and between elements (sometimes within the same shot but from different spectral planes) appears at an adequate confidence level for the spatially and temporally integrated data in this study. The plasma temperatures determined from the Al spectra indicate that increased input power produced increased plasma heating (PITHON shots PI2-PI4). At constant input power levels, higher Al-plasma temperatures have resulted from lower wire mass loading. For two shots PI5 and PI3, very similar Al spectra resulted when six and twelve wire arrays were fired while maintaining constant input power and mass loading. Also large shot-to-shot variations have not been observed in Al implosion spectra. Recent Al wire array data collected on BLACKJACK 4 have shown the expected 1s-2p resonance lines, thus substantiating their absence in the high input power shots from PITHON as being an experimental cutoff.

The results and questions that arise in the interpretation of the spectral data indicate need for upgrading the collection of the x-ray data. The greatest uncertainty regarding the plasma temperature and density estimates and the adequacy of the plasma transport model is the

-12-

spatial origin for the recorded spectral data. The most important next step is to collect spectra with spatial resolution together with simultaneous pinhole data through differential filters. The need for use of higher dispersive x-ray crystals such as PET or quartz is apparent from the well-resolved lines that were occasionally collected in higher order KAP data. Higher dispersion combined with spatial resolution will provide better diagnostics and better pictures of the plasma formation to improve the theoretical modeling and thereby refine the temperature estimates. The use of high-dispersive crystals also allows sufficient spatial separation of the He- and H-like resonance lines in Al and Ti that PIN or XRD active detectors instead of film can be placed behind the diffracting crystals to obtain temporal information concerning the formation of these ions in the plasma implosion.

References

1. C. Stallings, K. Nielsen and R. Schneider, Appl. Phys. Letter $\underline{29}$, 404 (1976).

2. C. M. Dozier, D. B. Brown, L. S. Birks, P. B. Lyons and R. F. Benjamin, J. Appl. Phys. $\underline{48}$, 3732 (1976).

3. Burton L. Henke and Eric S. Ebisu, Adv. X-Ray Analysis $\underline{13}$, 639 (1969).

4. D. B. Brown (to be published).

5. C. P. Bhalla, A. H. Gabriel and L. P. Presnyakov, Mon. Not. R. Astr. Soc. $\underline{172}$, 359 (1975).

6. J. Davis (to be published)

7. A. V. Vinogradov, I. Yu. Skobelev and E. A. Yukov, Sov. J. Quant. Electron. $\underline{5}$, 630 (1975).

8. B. F. Rozsnyai, private communication.

9. J. Davis, "Series Merging Technique," NRL Memorandum Report 2655, Oct. 1973.

10. P. G. Burkhalter, R. Schneider, C. M. Dozier and Robert D. Cowan, "Spectra of Mo XXXI-XXXIV from Exploded Mo-Wire Plasmas," (to be published) Preprint 108.

11. L. J. Roszman, "Dielectronic Recombination Rates for Heavy Ne-like Ions in Tokamak Type Plasmas," Bull. Am. Phys. Soc. $\underline{21}$, 1118 (1976), to be published.

12. B. F. Rozsnyai, J. Quant. Spectrosc. Radiat. Transfer $\underline{17}$, 77 (1977).

13. P. G. Burkhalter, C. M. Dozier and D. J. Nagel, Phys. Rev. $\underline{A15}$, 700 (1977).

Table I — Temperatures for exploded-Al-wire spectra

generator	shot	Expt. ratio 1s-3p/1s²-1s5p	Temperatures transport model		Expt. ratio 1s-2p/1s²-1s2p	Temperatures transport model		coronal	continuum
			thick	thin		thick	thin		
PITHON	PI1	2.4-2.9	525	750	0.60	575	850	700	500
	PI2	0.8	400	500	0.57	550	825	700	475
	PI5	2.2	500	700	N.A.*				500
	PI3	2.6	525	750	N.A.				525
	PI4	4.5	650	900	N.A.				N.D.
BLACKJACK	BL1	2.3-2.6	550	750	0.56	550	825	700	550

*N.A. (not available)

N.D. (not determinable)

Table II — Summary of Exploded-Wire Results

WIRES	MOST ABUNDANT IONIZATION STAGE	TEMP. T_e	MODEL	DENSITY N_e
Al	He or H	500-750	transport	1×10^{20}
		700	coronal	
		500	f-b continuum	
SiO_2	He	650	coronal	1×10^{20}
		400	recombining plasma	
Ti	Li or He	2.1	transport	6×10^{20}
		2.0	coronal	
Cr,Fe	Li	1.5	satellite lines	
Mo	Ne or F	2.5-4	coronal	$\sim 1 \times 10^{20}$

MULTI-WIRE
Al ARRAY

MAXWELL LABORATORIES

Al XII
$1s^2 - 1s2p \, ^1P$

Al XIII
$1s - 2p$

TRANSPORT
CODE TEMP.
750 eV

$1s^2 - 1s2p \, ^3P$

ELECTRON DENSITY
1×10^{20} el/cm^3

Al XIII
$1s - 3p$

Al XII
$1s^2 - 1s5p$

WAVELENGTH (Å)
4.0   5.0   6.0   7.0   8.0

ENERGY (keV)
3.0   2.0   1.5
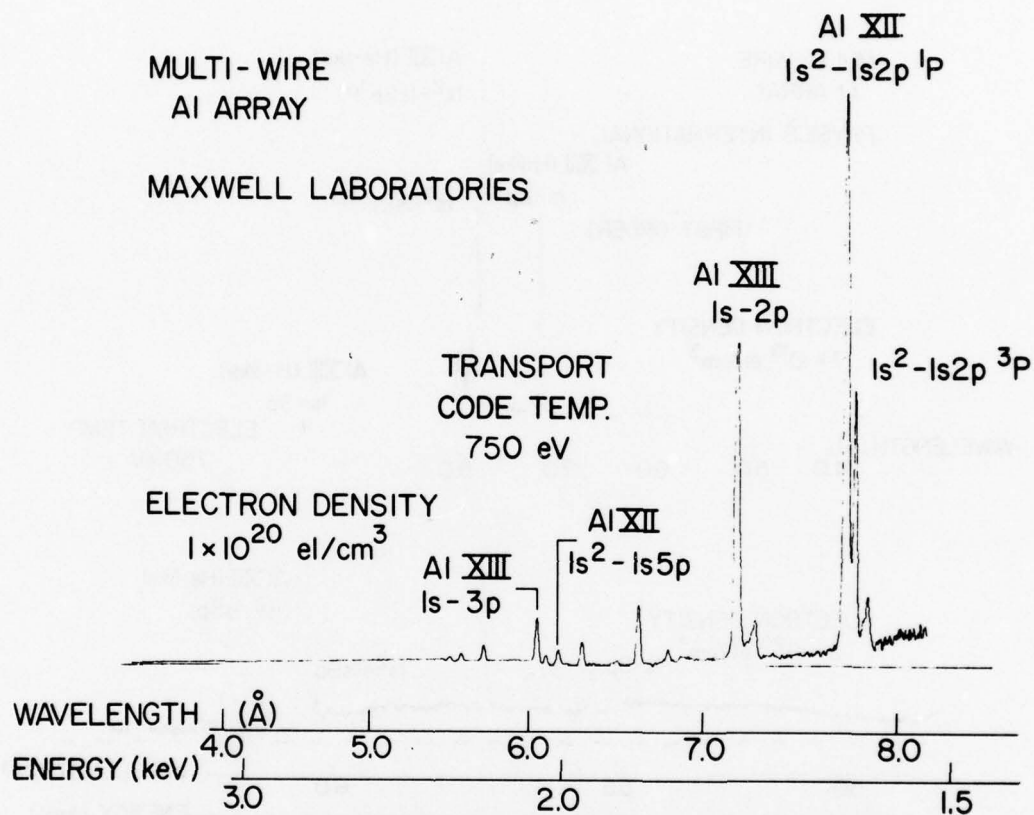
Fig. 1 - X-ray spectral emission of an exploded-Al-wire array
(shot BL1) from BLACKJACK 4. Spectral intensities were obtained
by processing the digitalized film densities for filter absorption,
No-Screen film sensitivity and KAP curved-crystal response.

17
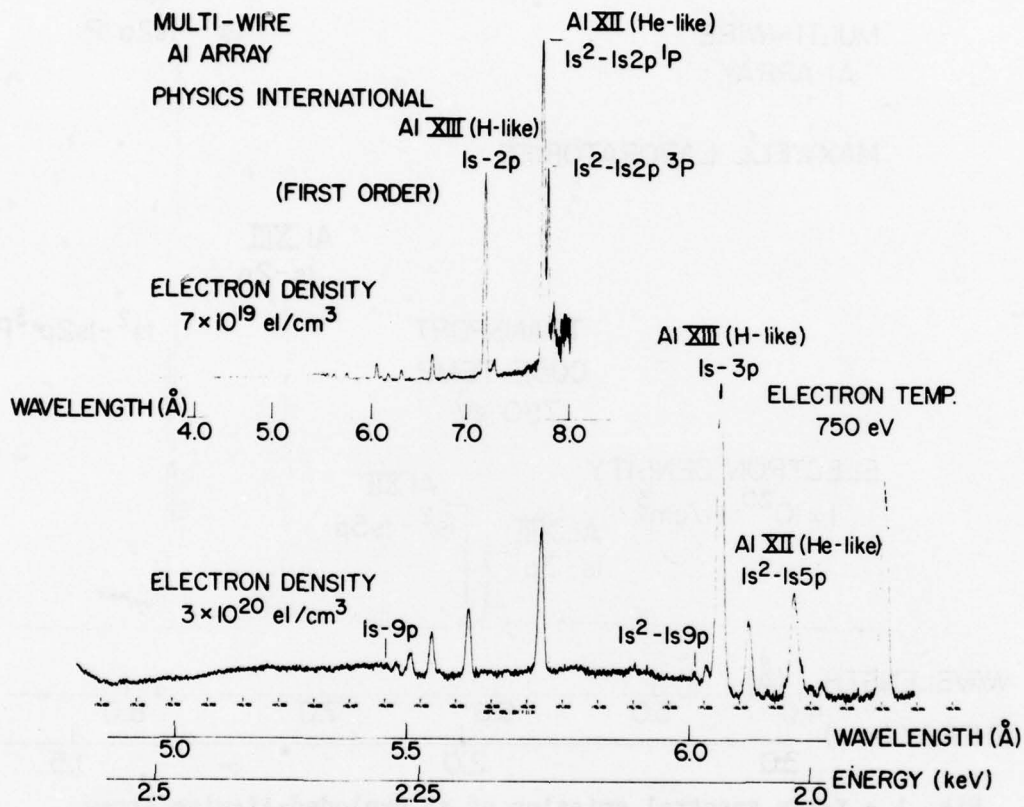
Fig. 2 - Al spectra intensities for PITHON shot PI1. The upper trace shows the entire first order Al spectrum while the bottom trace was diffracted from the (013) plane in KAP.

18
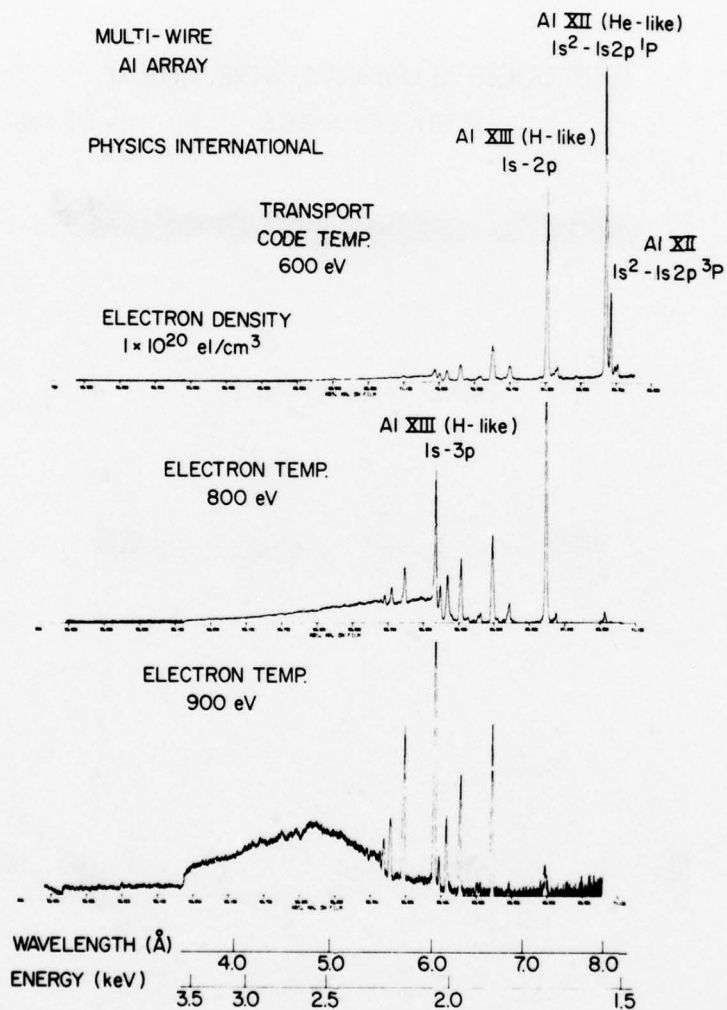
Fig. 3 - First-order Al spectral intensities for PITHON shots PI2 (top),
PI3, and PI4 (bottom) acquired from six-wire arrays.

EXPLODED-ALUMINUM-WIRE ARRAY

PINHOLE IMAGE $h\nu > 3\,keV$

DENSITY CONTOURS

CORE
$\leq 100\,\mu m$ $500\,\mu m$

INTERSECTION $\leq 100\,\mu m$
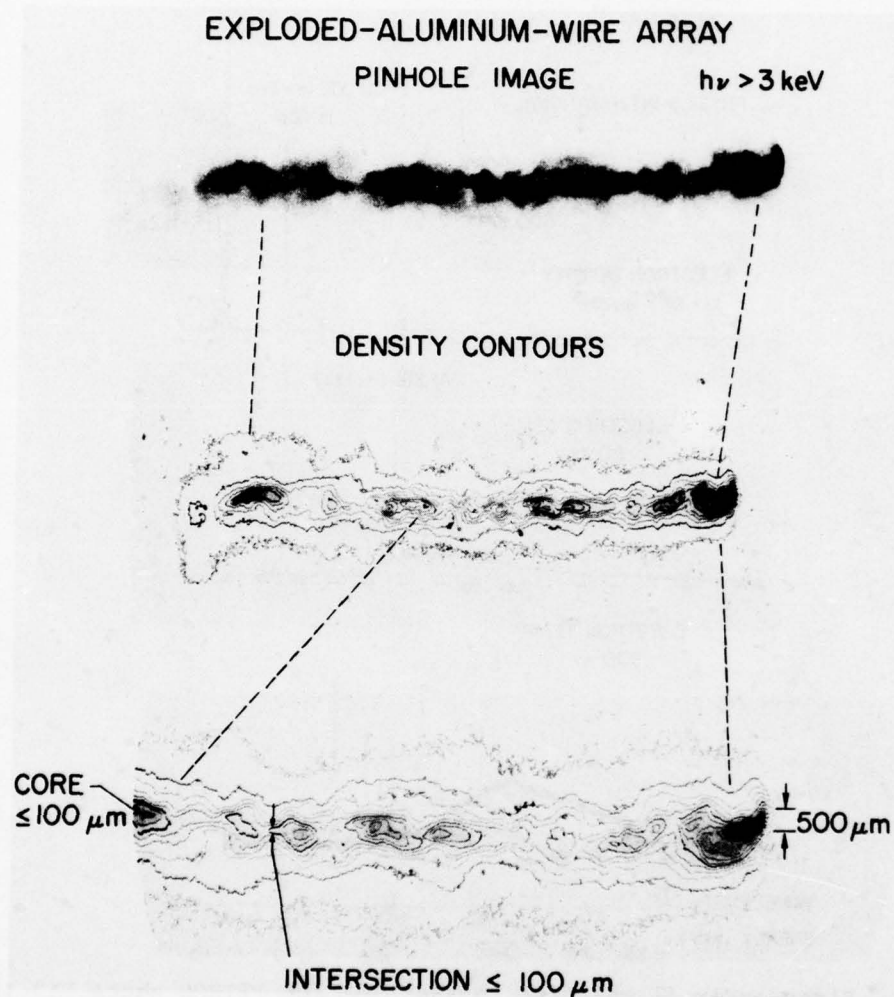
Fig. 4 - Pinhole image and densitometer contours of the image of a
12-wire Al shot PI5 on PITHON. Image was acquired through a $100\,\mu m$
pinhole. Each contour steps were set at intervals of 0.2 density
units. The x-ray image was acquired on the second Fine Grain Posi-
tive film. The plasma-implosion length was 3 cm.

20

PINHOLE IMAGE

DENSITY CONTOUR

500 μm
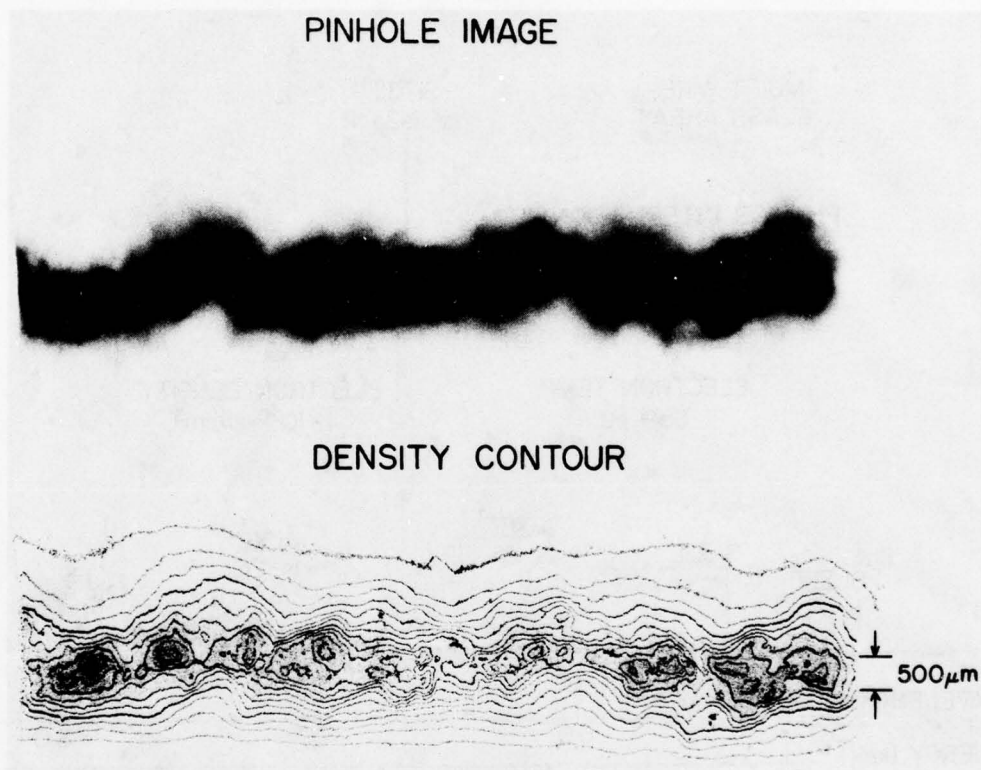
Fig. 5 - Pinhole image and contours for PITHON shot PI2. The image
was collected through an Al and mylar filter with a 50 μm pinhole.
The plasma-implosion length was 3 cm.

21
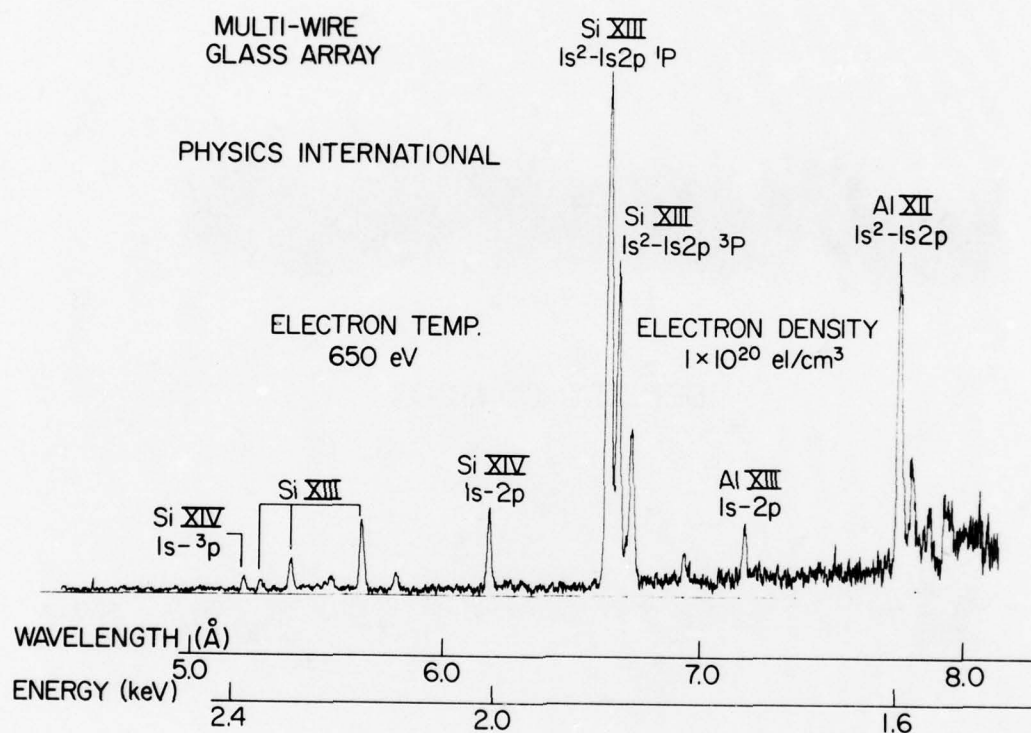
Fig. 6. - X-ray spectral emission from a glass
wire array shot PI6 on PITHON.
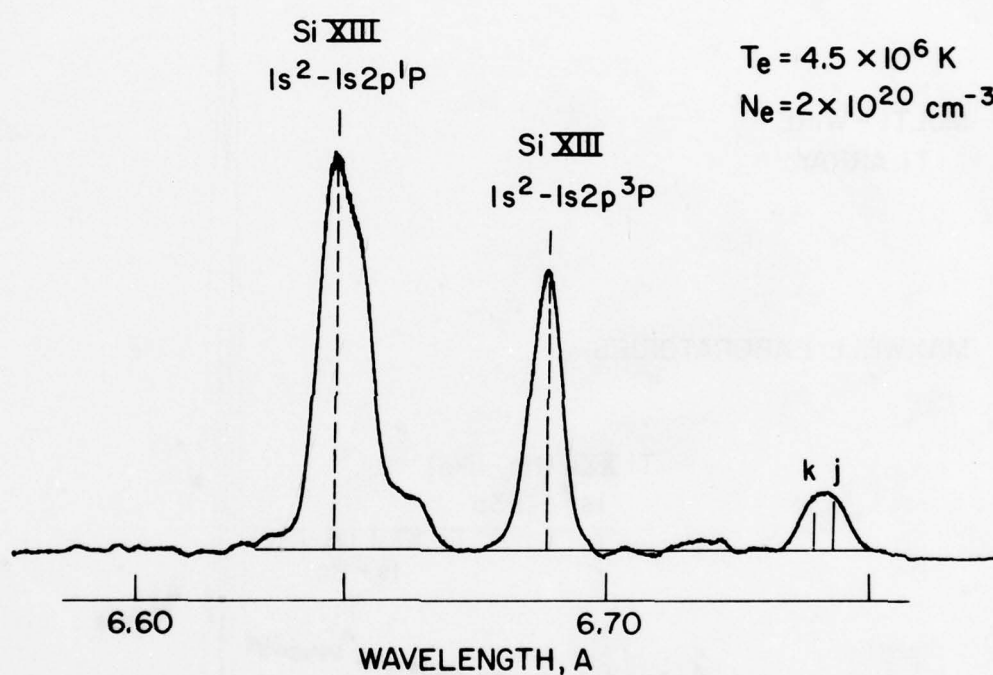
Fig. 7 - High dispersion KAP spectrum of the PITHON shot PI6 showing the He-like resonance lines in Si XIII. The satellites k, j formed mainly by dielectronic recombination are used for the temperature determination following the work in reference 5.
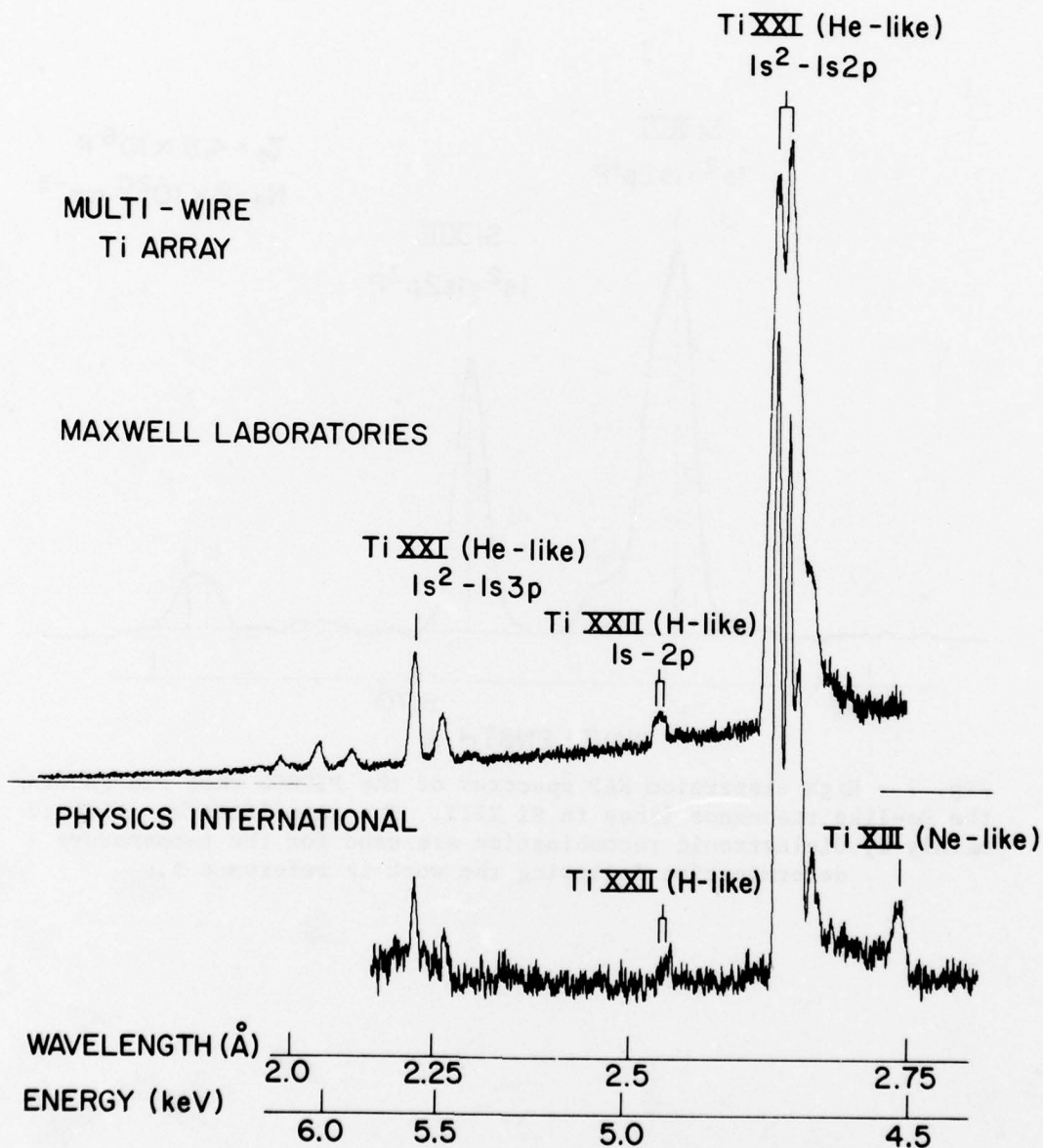
Fig. 8 - Ti spectra from BLACKJACK 4 and PITHON collected with
LiF curved-crystal spectrographs.
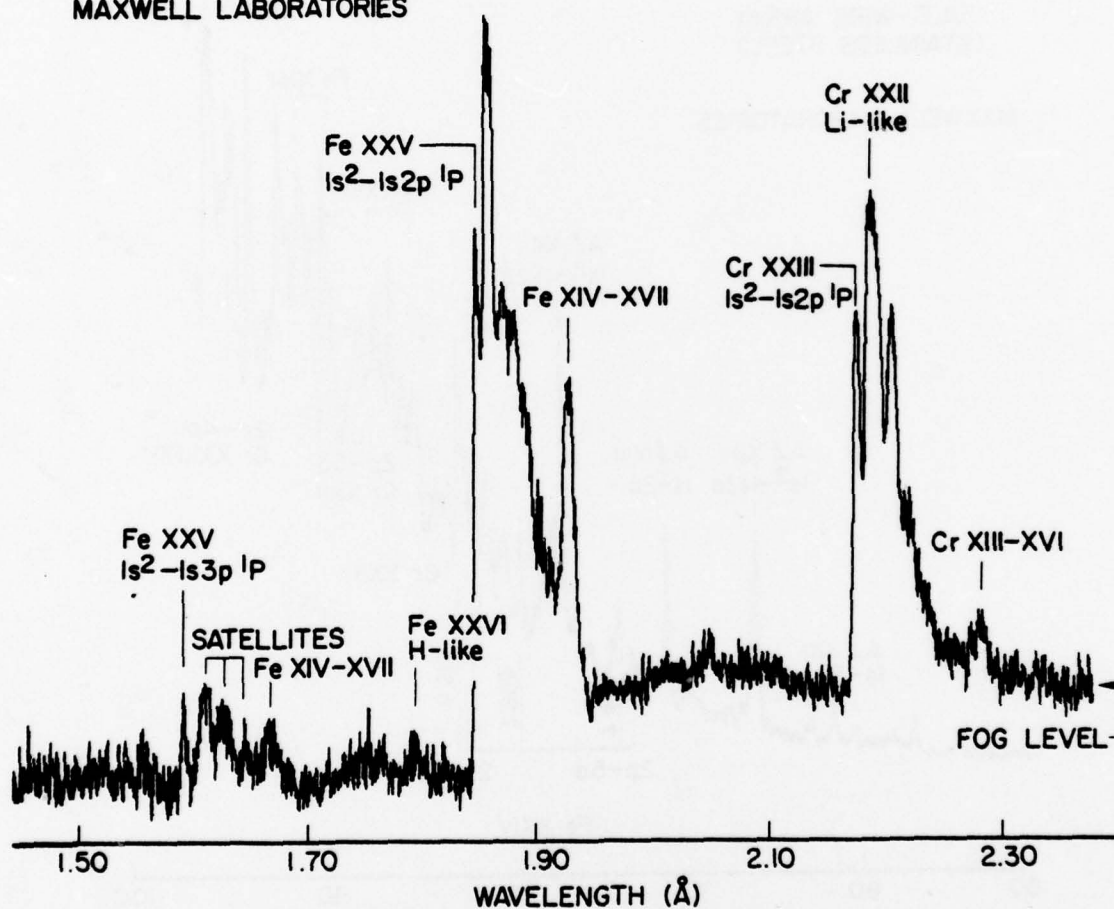
Fig. 9 - Fe and Cr K spectra acquired with the LiF crystal from shot BL3 on BLACKJACK 4.
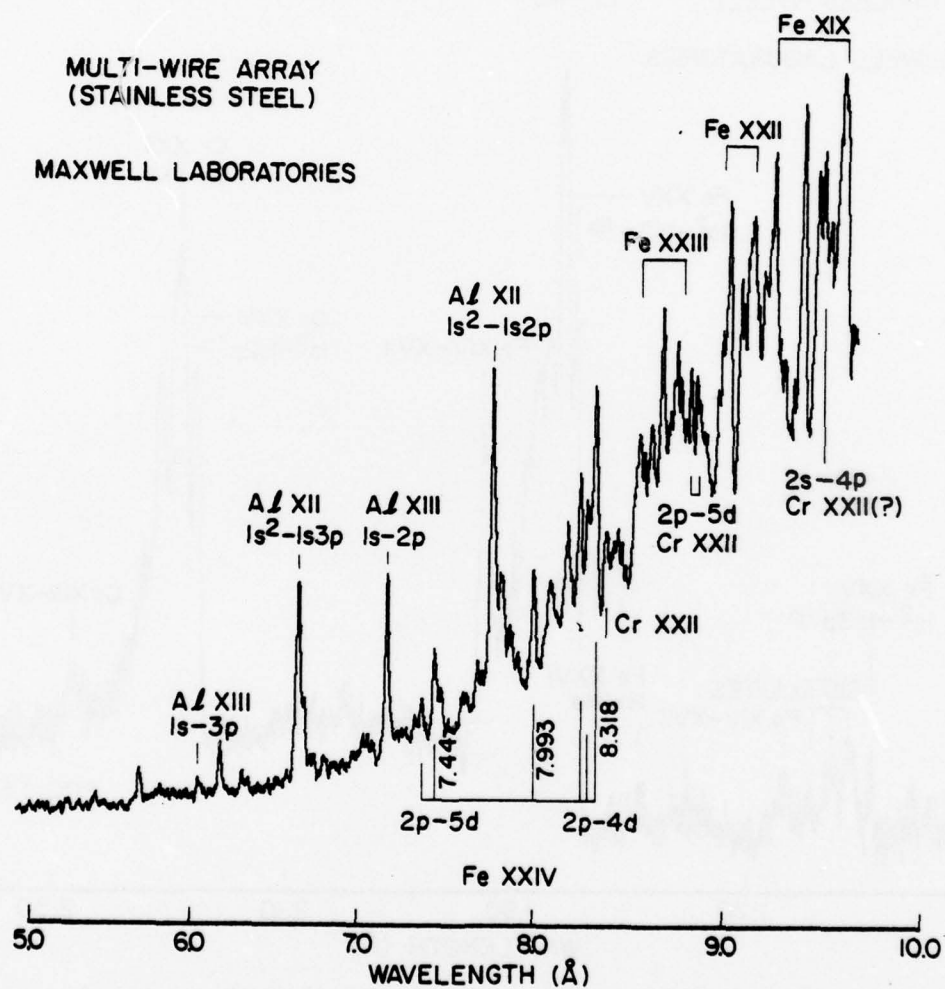
Fig. 10 - Stainless steel spectrum collected with the
KAP crystal shot BL3 on BLACKJACK 4.
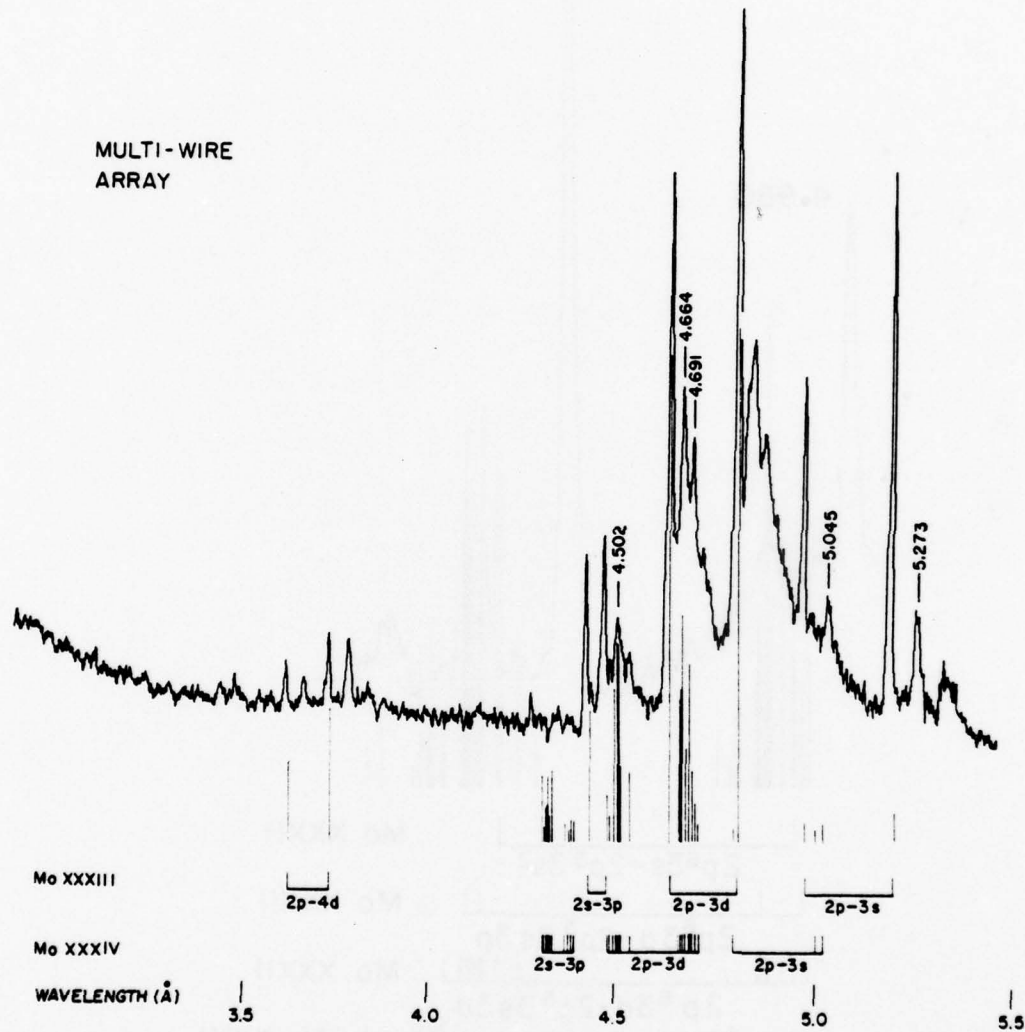
Fig. 11 - Mo spectrum from PITHON shot P18.
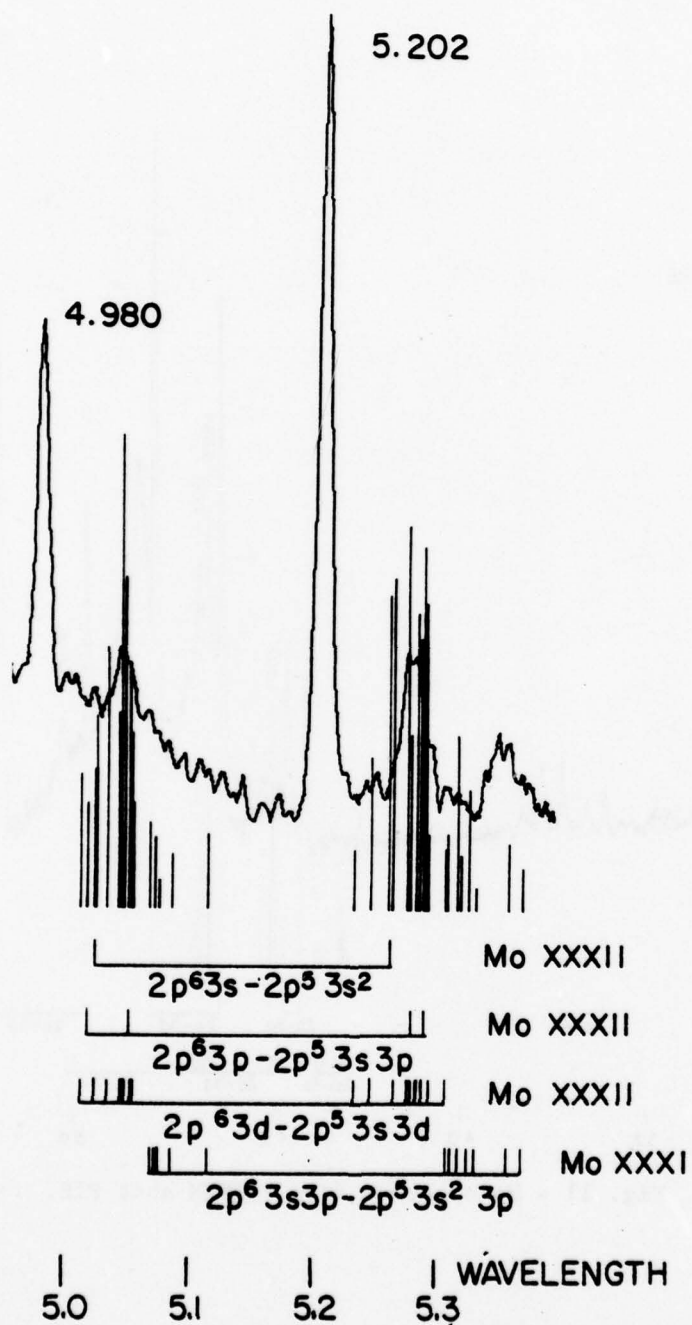
Fig. 12 - Calculated 2 p-3s satellite transitions near 5 Å compared with the multi-sire spectrum.

X-RAY SPECTRA FROM GAS-PUFF EXPERIMENTS AT PI *

I. INTRODUCTION

X-ray images and spectra from the gas-puff experiments conducted in the PITHON generator were examined and selected spectral films processed for data interpretation. Spectra from the inert gases Ne, Ar, Kr, and Xe were collected in the 1-5 keV region with convex, curved-crystal spectrographs using KAP, mica, and graphite diffraction crystals. Plasma temperatures in Ar data were obtained from spectral line ratios using a collisional-radiative equilibrium model. Plasma sizes have been obtained from densitometering various Ar and Kr pinhole images. The plasma temperature in Kr was estimated from the spectral distribution of ionization stages using the coronal model. The spectral patterns from Ne and Xe gas-puff shots indicated mixtures with other inert gases; and therefore, the interpretation for these two gases is preliminary.

II. EXPERIMENTAL

Pinhole images and spectra were collected from Ar-puff shots in series 887-890 in PITHON at low-to-medium power levels. Pinhole images of Ar plasmas were collected with 25, 50, and 100 μm apertures. Fig. 1 shows the images for shots 889 and 887. Linear scans were made across the images with a Joyce Loebl densitometer to determine the width of the plasma implosions. The implosion columns observed with the 100-μm pinhole appear to be somewhat uniform in emission between the electrodes, and in

* This section was co-authored with D. J. Nagel and R. Schneider.

shot 889 the emission extended to the 10-mil anode wire on the right side of the image. The images collected thru the smaller pinhole revealed regions of intense emission and a non-uniform plasma implosion. Fig. 2 shows two-dimensional densitometer contours of the 100 μm and a portion of the 50-μm pinhole images for shot 889. These contours define the intense regions of emissions to be about 100 to 250 μm in diameter. The width of the plasma implosion column varied between 500 and 1500 microns.

Another series of Ar puff-gas data was taken at higher input-power levels in shots from 930 to 956. Several pinhole images were examined in this series. The images were characterized by a higher emission intensity within the nearly collinear plasma column. The image for shot 940 (collected with a 50-μm aperture) is shown in Fig. 3. The pinhole image revealed a thin column of x-ray emission that more completely filled the inter-electrode spacing than in the previously shown images thru a 50 μm pinhole aperture. The diameter of the implosion column varied from 1500 μm on the cathode side to 500 μm near the anode wire. Therefore, the plasma size remained invariant with power input and the plasma column became somewhat more continuous in x-ray emission as the input power increased.

The Ar spectral data in the shots 887 to 890 were collected with a curved-graphite crystal in the 3-5 keV region. The Ar spectra shown in Fig. 4 for shot 889 were collected on Kodak No-Screen film. The spectral scans were made with a digital Grant densitometer. The spectrum on this shot was collected thru a 1/8-inch slit to provide spatial information. The slit was positioned perpendicular to the implosion column. The upper spectrum was scanned nearest the cathode side of the spectral line pattern. The He-like resonance line $1s^2 - 1s2p$ ^1P and the intercombination line

$1s^2$-$1s2p$ ^3P near 4 Å were over-exposed on this spectrum while they are observable on the lower spectrum. The lower spectrum was collected from near the anode thru a 12.5-μm Al filter.

III. RESULTS-ARGON

Plasma temperatures and densities were determined from line ratios of closely-spaced lines in the Ar spectra. Line ratios as a function of electron temperature were calculated for the He-like $1s^2$-$1s5p$ line and the H-like $1s$-$3p$ line. These lines are adjacent and closely spaced with x-ray energies at $\sim$ 4 keV. Both are identified in the upper spectrum in Fig. 4. In that spectrum (cathode side), the $1s$-$3p/1s^2$-$1s5p$ ratio was 1.15 while it was only 0.5 in the lower spectrum (anode side). This indicates a hotter plasma on the cathode side. The intensity ratio calculations were made with a collisional-radiative equilibrium transport model (C.R.E.) for plasma volumes of 50, 100, and 250 μm in diameter at an ion density of 1×10^{20} cm^{-3}. The hotter spectrum formed near the cathode had a C.R.E. temperature between 1.1 and 1.3 keV for implosion sizes of from 250 to 100 μm respectively. The spectrum from near the anode had a plasma temperature between 0.9 and 1.05 keV for the same 250 to 100 μm plasma size variation. Temperature higher by 150 to 200 eV would be derived if calculations for 50 μm spots were used with the measured ratios. For these lines in Ar, the opacity corrections are small. The $1s$-$3p$ line is thin and the optical depth is only $\sim$ 1-2 for the $1s^2$-$1s5p$ line. The density of the plasma was estimated from the ^1P to ^3P line ratio of the He-like resonance and intercombination lines. These lines are adjacent in wavelengths with values near 4 Å. As shown in Fig. 4, they are over-

-31-

exposed in the cathode-side data but useable in the anode-side spectrum.
An electron density of 2×10^{21} cm^{-3} was found for the plasma near the
anode side.

An Ar spectrum collected without spatial resolution and recorded with
the less sensitive Type-T x-ray film is shown in Fig. 5 for shot 890.
The 1s-3p and 1s^2-1s5p lines have about equal intensities, implying a
plasma temperature range of 1.0 to 1.2 keV based on the C.R.E. model.
The ^{1}P to ^{3}P line ratio again yields a plasma density of $\sim 2 \times 10^{21}$
el/cm^3.

Ar spectra collected in second-and third-order diffraction with a
mica crystal (supplied by NRL) are shown in Fig. 6 for a high-input-power
shot 944. Because of the high emission level, the He-like 1s^2-1s2p ^{1}P
resonance line was overexposed in third order; however, the ^{1}P to ^{3}P line
ratio could be determined in the second-order spectrum yielding a plasma
density of 7×10^{20} el/cm^3. The Ar XVIII to Ar XVII line ratio in the
third-order spectrum corresponded to a plasma temperature of 1.3 to 1.45
keV for shot 944.

IV. KRYPTON-EXPERIMENT AND RESULTS

Pinhole images from Kr shots revealed plasma implosion and energetic
x-ray emission. Fig. 7 shows the plasma images for shot 968. The top
image was collected on the front film (Kodak Fine-Grain Positive) while
the second film (Kodak type-T) was placed behind the first film. The
front film served as a thick filter and transmitted x-rays with energies
> 3.6 keV. Since the Kr spectrum from the thermal plasma has energies
< 3 keV the faint broad plasma column in the second film image arises

-32-

from inner-shell emission (K lines) from the Kr plasma. Also it is seen that the anode wire is a source of energetic x-rays. The broad plasma column (~ 4000-μm wide) extends across the inter-electrode spacing viewed by the pinhole camera. The implosion column of thermal x-rays viewed in the front film is somewhat more irregular in Kr than for Ar. The Kr hot plasma column has a diameter of 1500μm and extends only part way in the inter-electrode spacing in this shot.

The puff-gas experiment is capable of producing highly-ionized Kr spectra. Fig. 8 shows the Kr spectrum from the high-input power shot 968 collected with the mica-crystal spectrograph. The Kr L-series spectrum is dominated by transitions in Ne-like Kr XXVII. Weak Na-like satellite transitions can be observed on the long-wavelength side of the 2p-3s transitions at ~ 7.4 and ~ 7.6 Å. The spectral region between ~ 6.0 and 6.6 Å contains F-like transitions in Kr XXVIII together with the two 2s-3p transitions in Kr XXVII. The observed distribution of ionization stages yields a plasma temperature of 1.5 keV based on the coronal model. In the preceeding shot 967 a 50% Ar-50% Kr gas mixture was excited. The Kr and Ar lines were intense in this shot because No-Screen film was used instead of type T, and therefore more of the weaker line structure was visible. However, the distribution of ionization stages in Kr was the same as in shot 968. The temperature for the Ar plasma in shot 967 was 1.0-1.2 keV based on the 1s-3p/1s^2-1s5p line ratio and C.R.E. calculations.

V.   XENON AND NEON-EXPERIMENTAL AND RESULTS

The spectral data and interpretations for Xe and Ne are preliminary in nature and more work is necessary to complete the spectral analysis

for these gases. Shots using Xe gas were found to produce weak spectra of either Ar or Kr gas. A faint Kr spectrum and an unknown spectral pattern was recorded for shot 981. By comparing spectra from different shots, the first-order 2p-3d, 3s lines and the second-order 2p-4d, 5d, 6d lines in Kr XXVII were identified. Since a highly-ionized Xe spectrum is unknown and little spectroscopy work is available for this portion of the periodic table, pattern recognition for Xe was not possible. In order to interpret the Xe spectra, wave-lengths for transitions in likely-ionization stages (those near closed-shells) such as Ar-like ions were performed with a relativistic Hartree-Fock program. The calculated wave-lengths for Ar-like Xe XXXVII and Al-like Xe XLII agreed with the faint line structure in shot 981 shown in Fig. 9. Even though additional lines in the pattern remain unknown, ionization stages including those identi-fied above occurred in this gas puff shot. The plasma temperature to generate these ionization stages in Xe is 2-2.5 keV based on the coronal model.

The spectra examined from the Ne-gas-puff shots were found to be lacking in completeness. A densitometer trace of a faintly-recorded Ne-spectrum is shown in Fig. 10. The He and H resonance lines are distinct in this spectrum. Model calculations for Ne plasmas are currently under-way. In other shots (976-978) the higher Rydberg transitions and their satellites were visible. The patterns were complex and exhibited shot-to-shot variation. There is some suggestion for possible line splitting but this will require further study.

-34-

VI. DISCUSSION

The plasma temperatures and densities in the gas-puff data are comparable to those found in exploded wires. For Ar plasmas in the puff data the C.R.E. model gave temperatures generally between 1.0 and 1.4 keV. The distribution of ionization stages in Ar yields a coronal temperature of ~ 1 keV. This plasma temperature is comparable to the 1.1 keV coronal temperature found in exploded-wire data for Cl. The distribution of ionization stages found in Kr indicates a higher coronal plasma temperature (1.5 keV) than was found for the Ar puff-gas plasmas. This is consistent with exploded-wire data in which the plasma temperature increases as a function of atomic number with exploded-iron wire plasmas having a temperatures of 1.4 keV. The He-like line ratios gave a plasma density of ~ 2×10^{21} el/cm^3. It was observed that the higher Rydberg transitions were distinct to the 1s-8p line in Ar XVIII and 1s^2-1s8p in Ar XVII, which yields the same density value by the series merging technique. This density (of 2×10^{21} el/cm^3) is about the same as found in exploded single-wires in which high-density spots are formed by the z-pinch mechanism. The 100 to 250 μm diameter regions of intense x-ray emission, observed in the Ar plasma images, are of comparable size to the pinches in exploded wires.

Several combinations of x-ray films and diffraction crystals, both with different sensitivities, were employed in recording the spectra. Variations in x-ray emission from the plasma implosions from different spectral wavelengths require unique spectrograph combinations in order to cover the wide range of atomic numbers for the inert gases. The high x-ray intensity from Ar gas implosions and the high

-35-

diffraction efficiency of the graphite crystal required thick absorber foils to avoid overexposure. This complicates the data reduction to obtain accurate line intensities. Kodak type-T film has a smaller grain size than No-Screen film and was known to be about 15 times less sensitive than No-Screen film at high x-ray energies ($>$ 8 keV). This is about the best level of exposure reduction in order to record readable Ar and Kr spectra. The spectral intensities shown in this report were obtained using the relative film response for No-Screen film. Subsequent to processing the spectral data, Dennis Brown at NRL calculated the H and D film response for type T film for x-ray energies down to a few keV. The calculated response for type-T film was found not to be significantly different from the measured response function of No-Screen film in the 3-4 keV region. The line ratios for the closely-spaced lines used for the temperature and density determination are largely unaffected by uncertainties in the film and crystal responses and in absorption coefficients for the filters. However, the Ar spectra will be reprocessed to obtain the complete spectral intensities using the available calculated response function for type-T film.

The use of a curved-mica crystal was beneficial for recording Ar spectra because of its lower efficiency as compared to graphite or KAP and because the third-order diffraction plane gives good spectral resolution. Actually the 2d-spacing for third-order mica is nearly the same as for graphite, but the line widths are narrower for mica because of the mosaic structure of graphite crystals. The curved-mica diffracting crystal plus type-T film combine to allow collection of readable Ar data. Most of the second- and third-order Ar spectral lines are resolved and at a proper exposure level.

More intense and complete spectral patterns for Xe and Ne are needed. Spectra for both elements occur in the 9-18 Å wavelengths region. To obtain more intense spectral lines, the use of thinner light-tight windows and the KAP crystal are indicated. Since the features of these spectra are unknown, shots with trace amounts of impurities with known spectral wavelengths are recommended to provide wavelength calibration. The Xenon spectrum could be calibrated with a weak overlapping Ne spectrum. Also Ar spectral lines collected in third-order with the mica crystal could serve to calibrate a portion of the Xenon spectrum.

Another area for further study is the collection of Ar puff-gas spectra thru small slits for spatial information. Correlation of the spatially-resolved spectra with pinhole images should allow improved temperature estimates compared to the ranges presented in this work. The determination of possible variations of plasma temperature and density along the Ar implosion would allow better modeling of the gas-puff plasma formation.
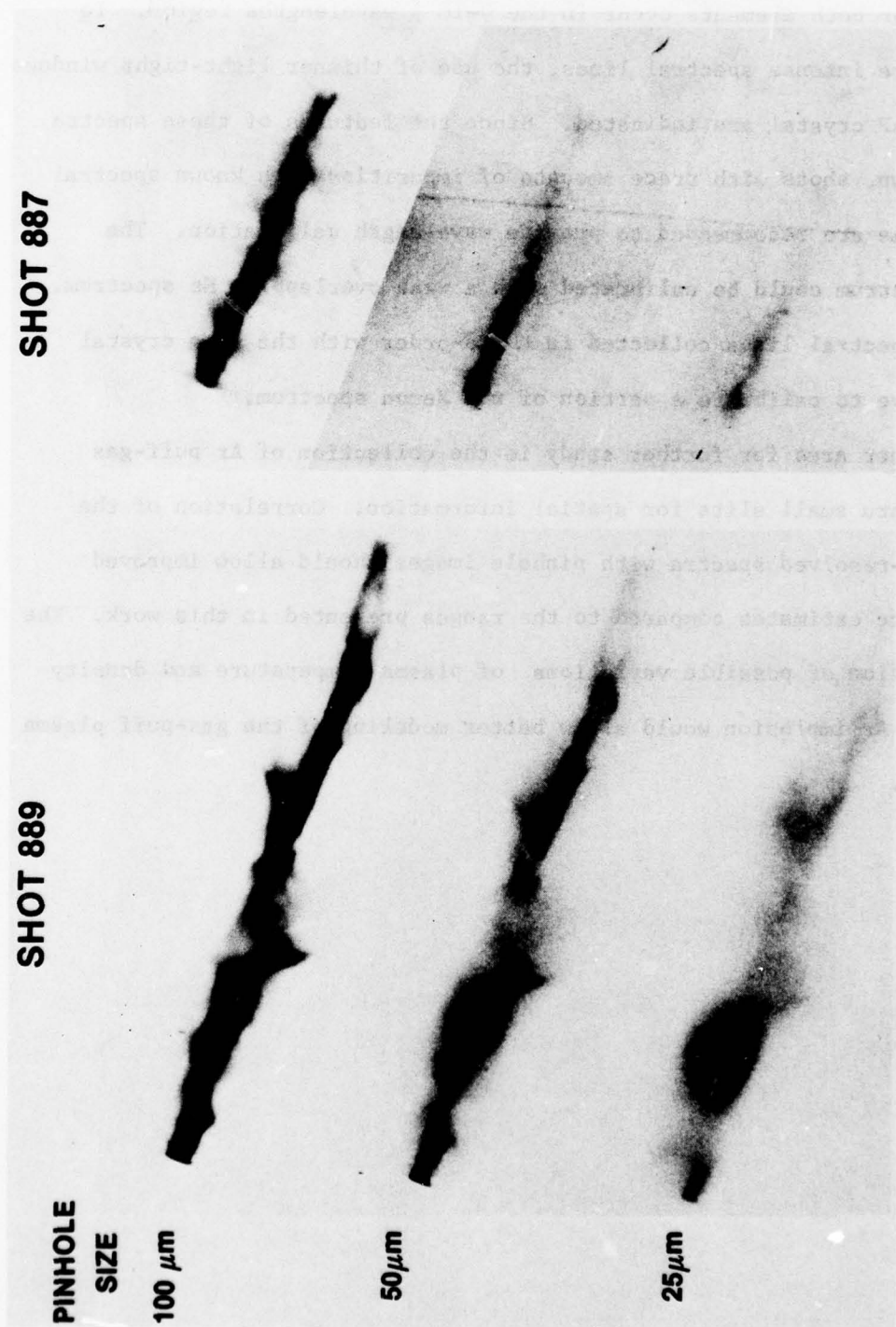
Fig. 1 - Pinhole images for Ar plasmas shots 889 and 887. Plasma columns are terminated by the 10-mil anode wire on the right side of the images and obscured by a housing that blocks the view of the plasma within 3/4-cm of the cathode on the left side of the image. The visible portion of plasma is 4.3 cm in length in shot 889 and 2.1 cm long in shot 887.
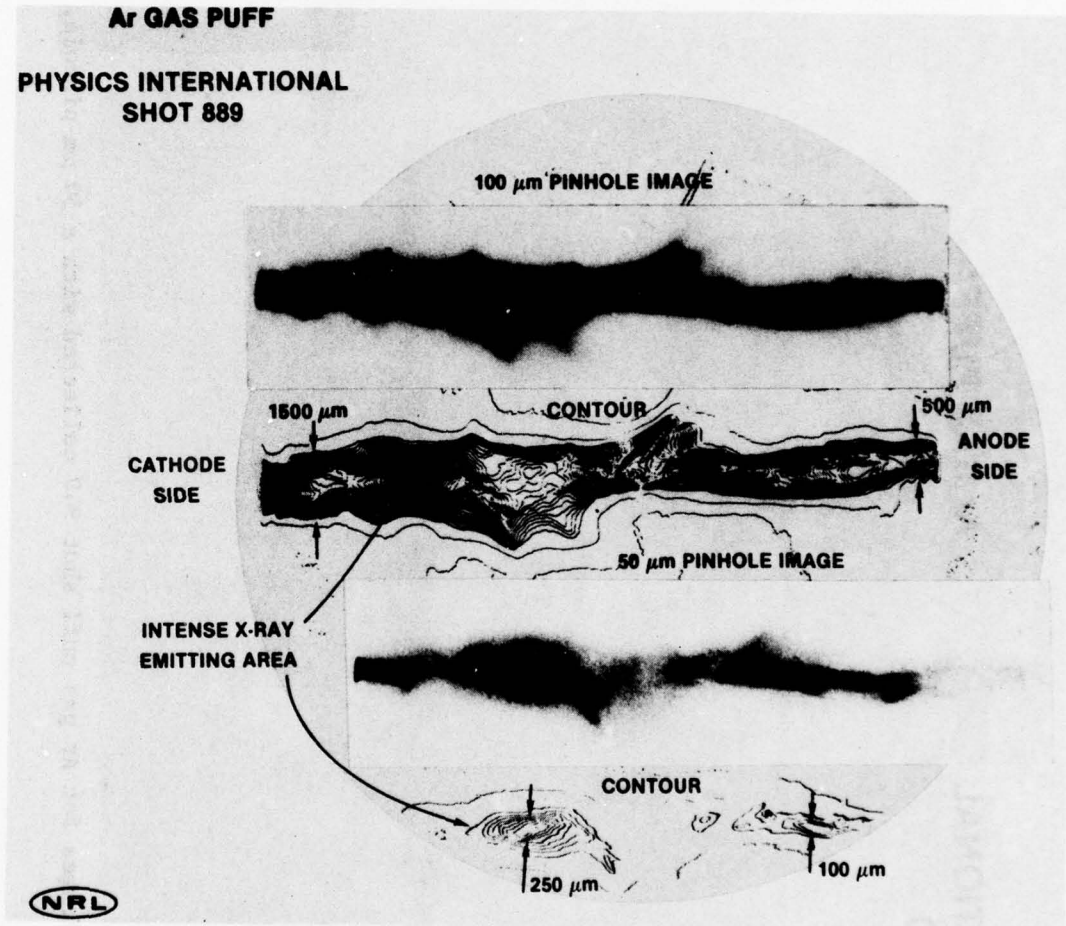
Fig. 2 - The images for shot 889 are shown again for the 100 and 50- m apertures together with 2-D densitometer contours. The size of the plasma column is indicated in the more dense contour of the 100 μm image while the localized intense emitting regions are found in the contours of the 50 μm pinhole images.

PHYSICS INTERNATIONAL   Ar GAS PUFF
Ar SHOT 940

50-μm PINHOLE IMAGE
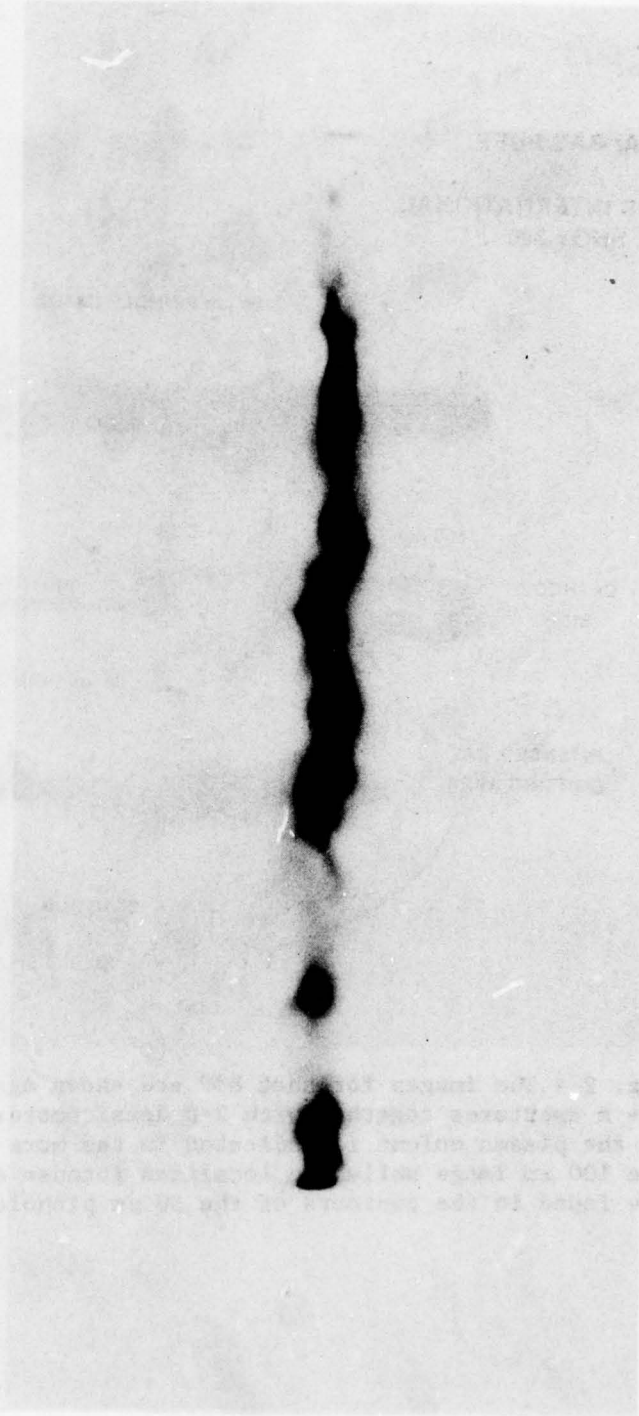
Fig. 3 - Plasma images for Ar gas puff shot 940 collected with a 50 μm pinhole.
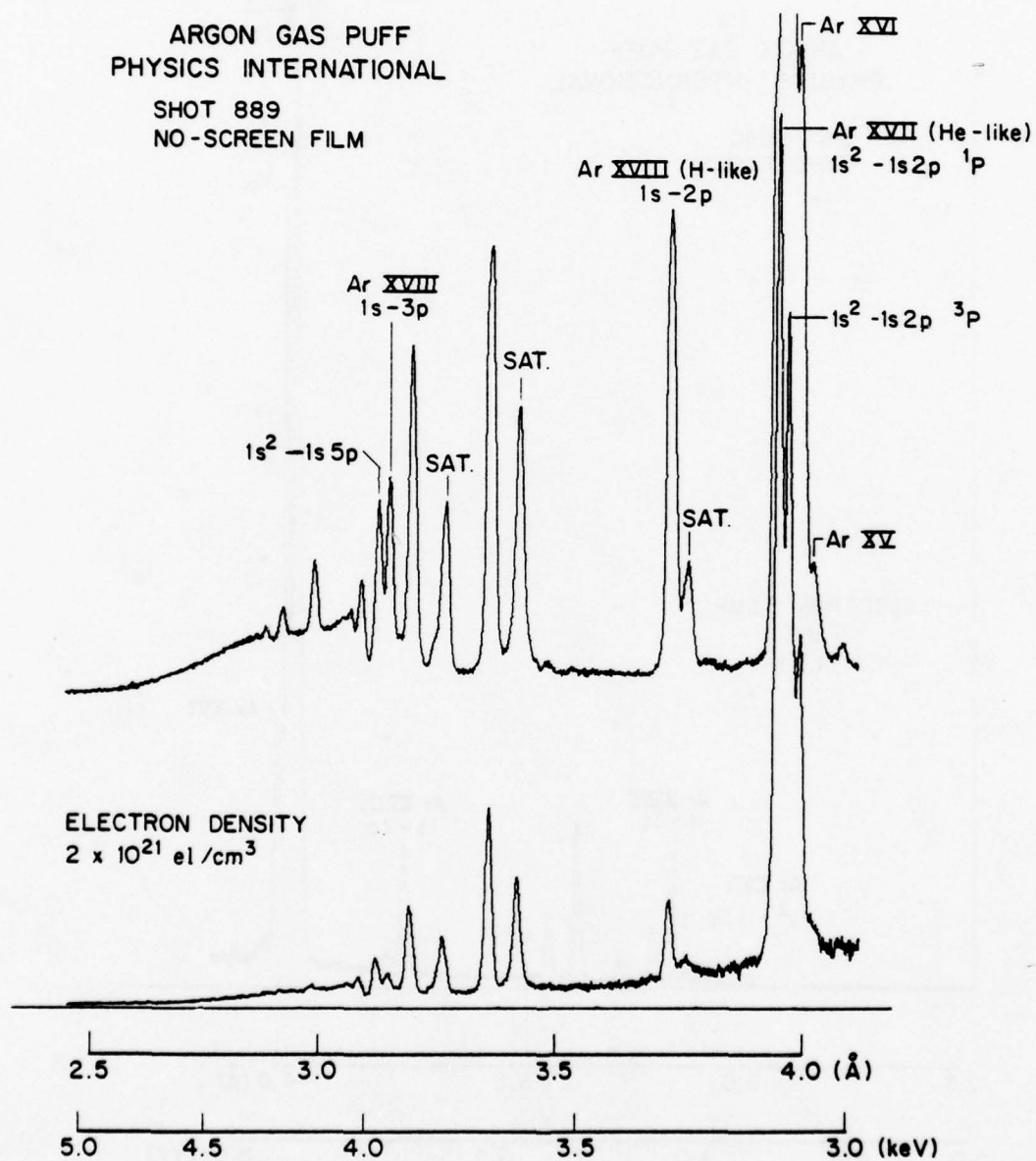
Fig. 4 - Ar x-ray spectrum for shot 889.

-41-
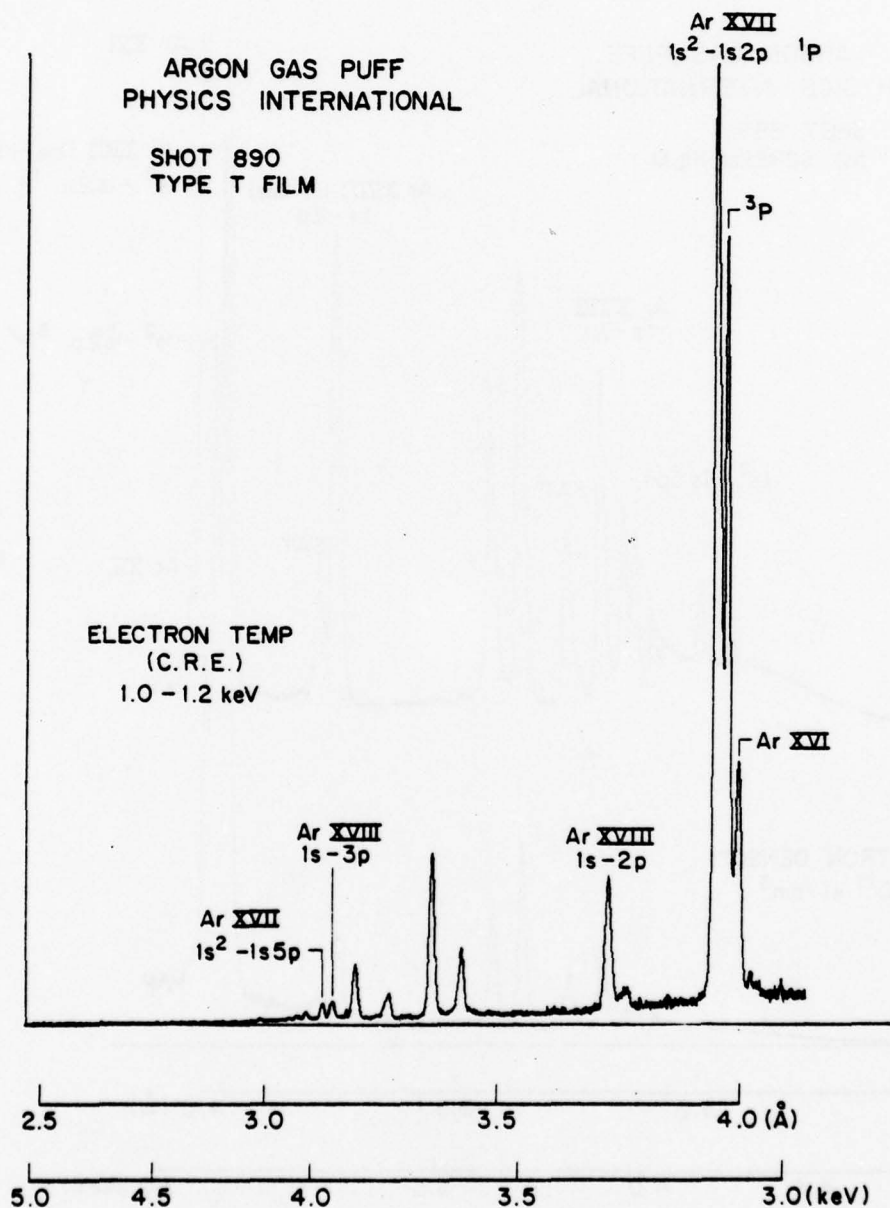
Fig. 5 - Ar spectrum for shot 890.
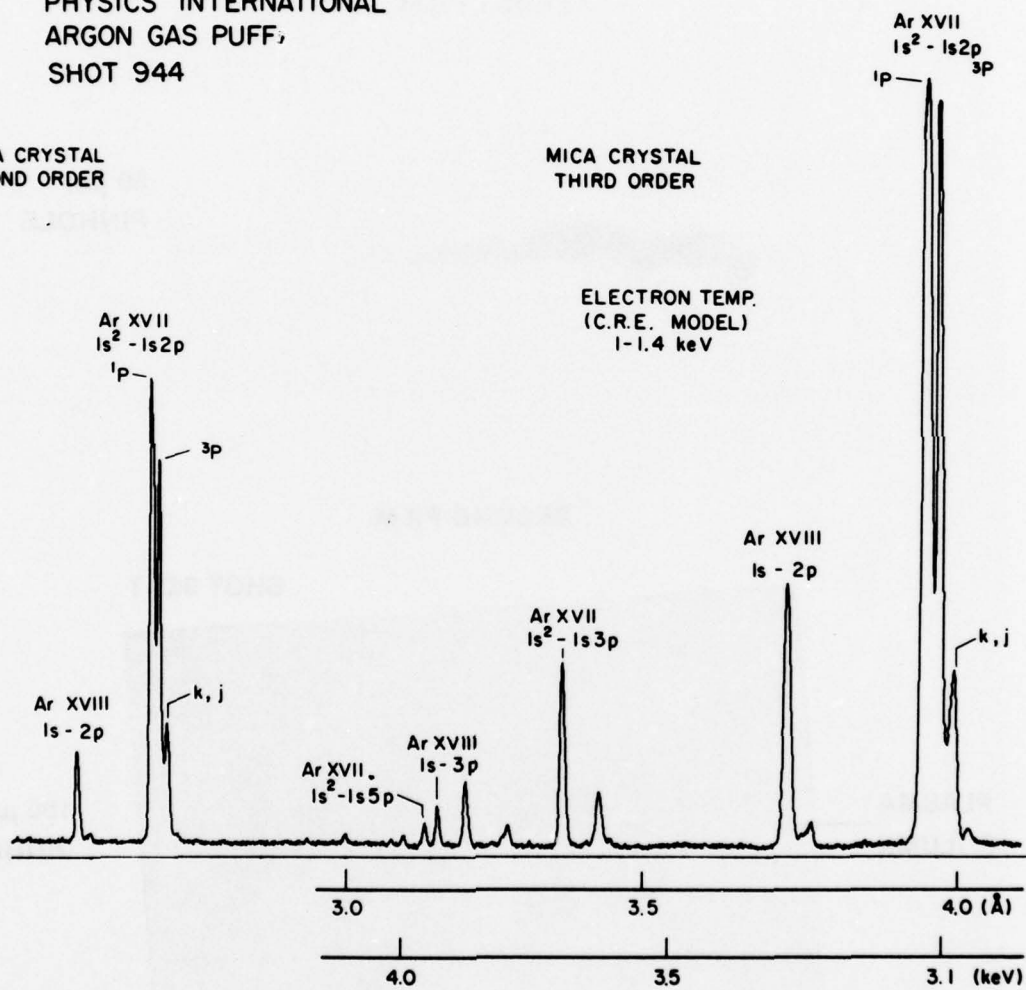
Fig. 6 - Ar spectrum for shot 944.
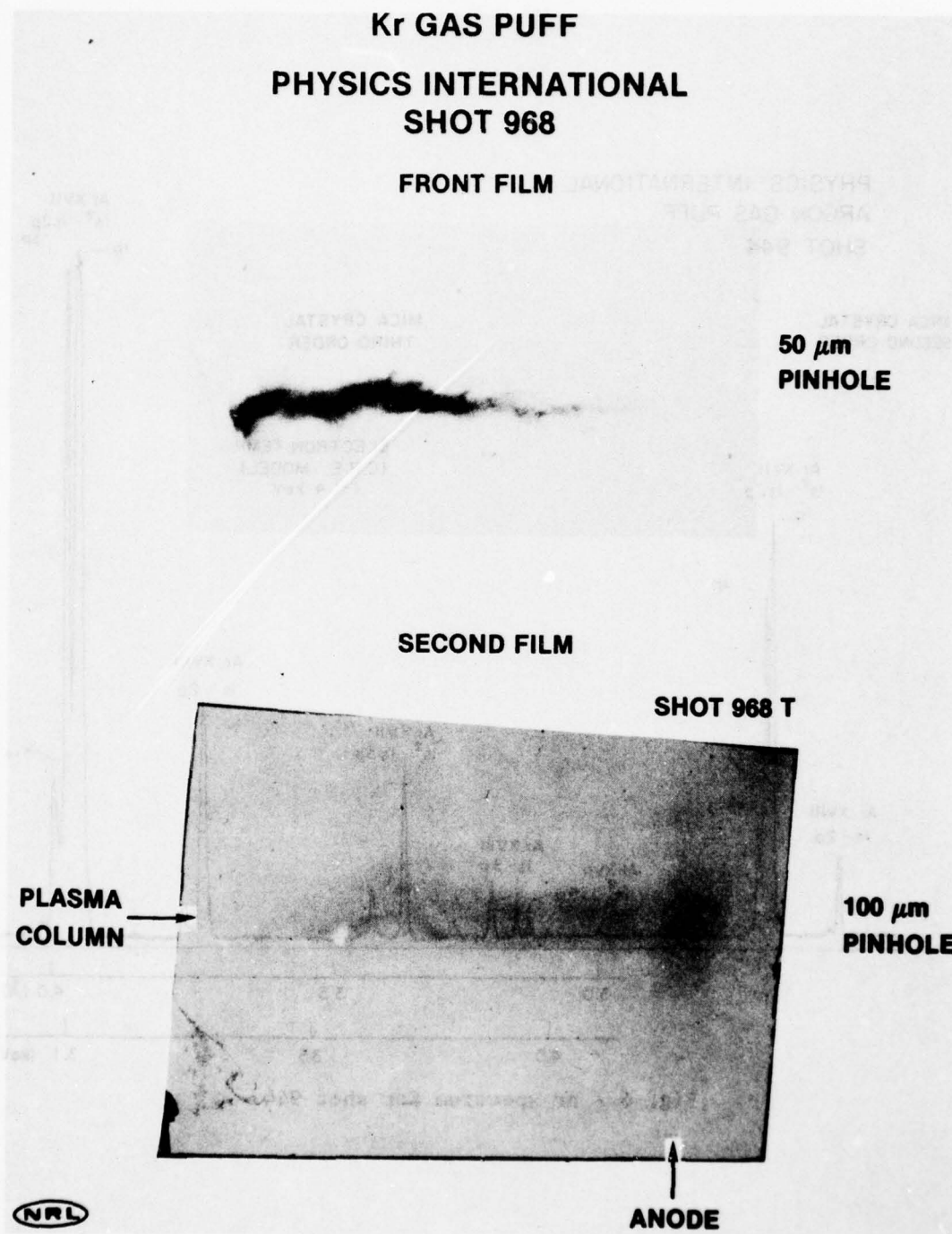
Fig. 7 - Pinhole images for Kr shot 968.
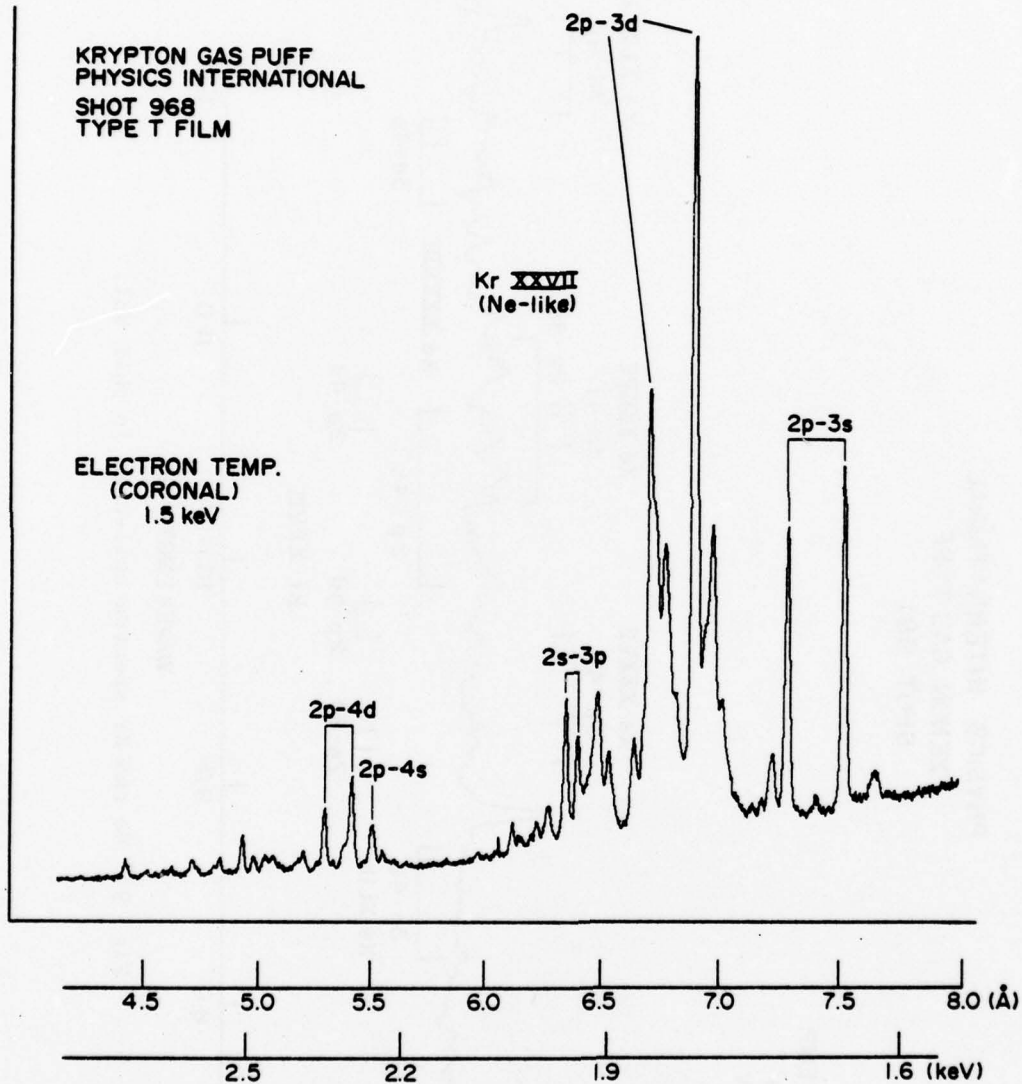
Fig. 8 - Kr spectrum for shot 968.
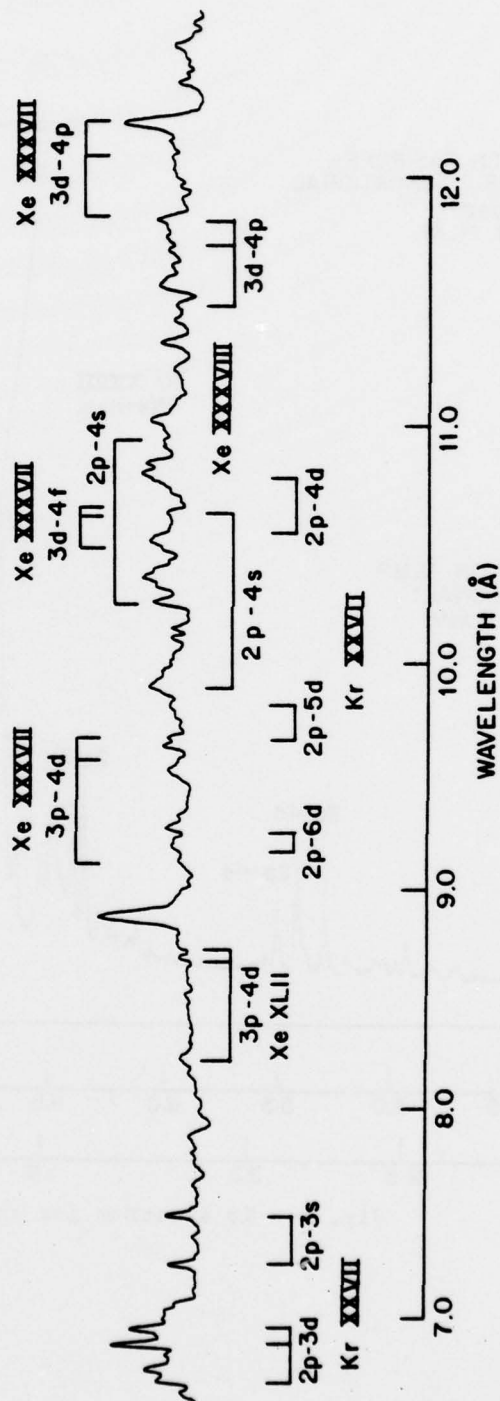
Fig. 9 - Xe and Kr spectra collected in shot 981.

PHYSICS INTERNATIONAL

NEON GAS PUFF

SHOT 970
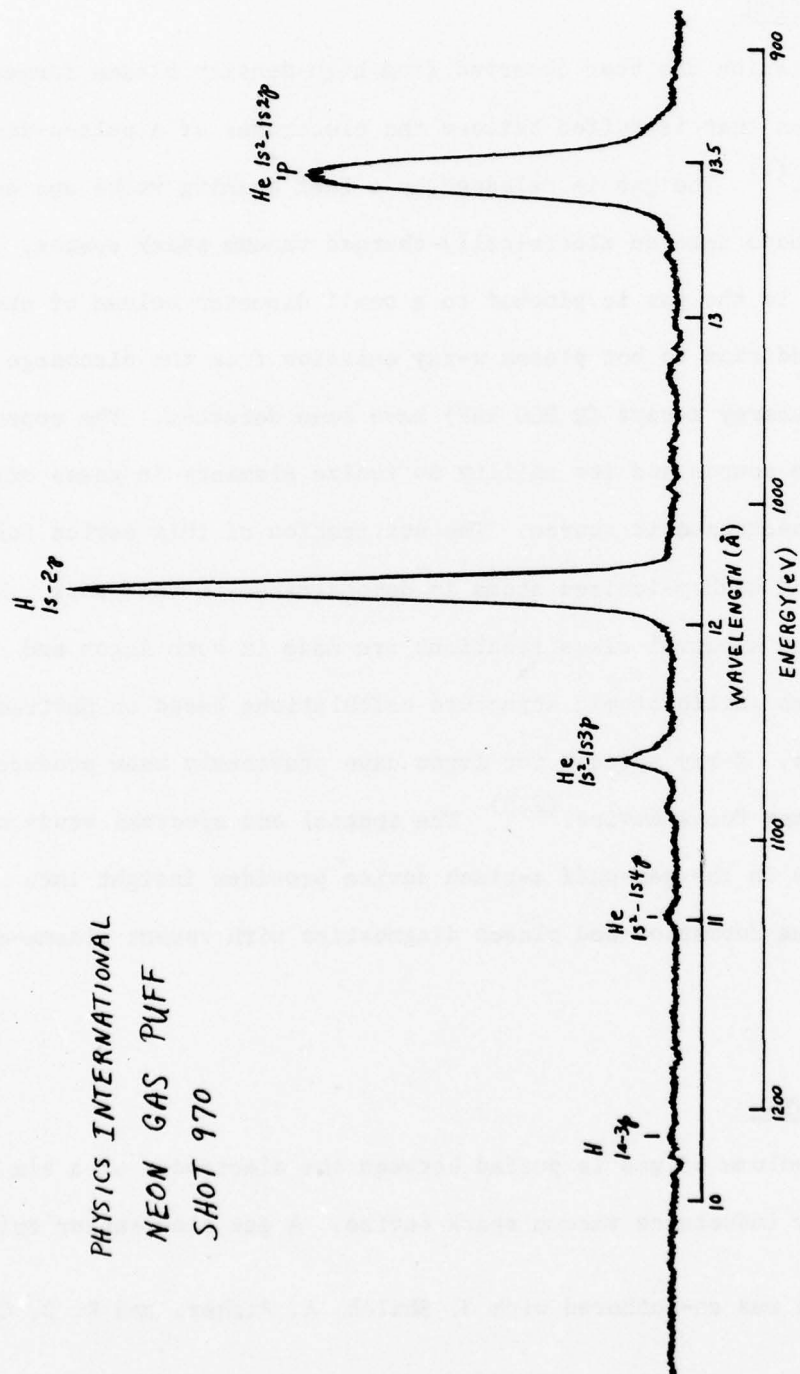
Fig. 10 - Ne spectrum in shot 970.

X-RAY SPECTRA FROM A GAS-PUFF Z-PINCH DEVICE *

I. INTRODUCTION

X-ray emission has been observed from high-density plasma formation
produced by gas that is puffed between the electrodes of a pulsed-dis-
charge device.[1] The gas is released by a fast opening valve and enters
through the anode into an electrically-charged vacuum spark system. The
plasma formed in the gas is pinched to a small diameter column of about
100 μm. In addition to hot plasma x-ray emission from the discharge
cclumn, high energy x-rays ($\geq$ 200 keV) have been detected. The reproduc-
ibility of the source and its ability to ionize elements in gases offers
a potential spectroscopic source. The utilization of this device for
spectroscopy of highly-ionized atoms is demonstrated in this work. New
wavelengths and spectral classifications are made in both Argon and
Krypton with ab initio atomic structure calculations based on Hartree-Fock
wave functions. X-ray spectra for Argon have previously been produced in
the dense plasma focus device.[2,3] The spatial and spectral study of Ar
x-ray emission in the gas-puff z-pinch device provides insight into
imploded-plasma formation and plasma diagnostics with recent plasma-model
calculations.

II. EXPERIMENTAL

A small volume of gas is puffed between the electrodes of a six
capacitor, low inductance vacuum spark device. A gas flow sensor triggers

* This section was co-authored with J. Shiloh, A. Fisher, and R. D. Cowan

an electrode that is used to initiate the electrical discharge. The gas is puffed from a fast opening valve[4] through the anode. The valve chamber is charged with about 20 cm^3 of gas at a pressure of five atmospheres. The anode used in this spectral study produced a hollow cylinder of gas about 4 cm in diameter and a few mm thick. By adjusting the injector diameter and the pressure of the injected gas, the time of the plasma collapse can be set to coincide with maximum current in the system and thereby achieve efficient energy conversion in the discharge. In the present study, a 12 μF capacitor bank consisting of six cylindrical capacitors in a circular array was used at a charging potential of 30 kV. The current rises to 300 kA in about 1.5 μs. An electrode spacing of 9 mm was found to be optimum for generating reproducible plasma implosions - reproducible in the sense that intense pinches are formed in every shot with a jitter in time of 10 ns. The thermal plasma has a lifetime of $\sim$ 20 ns and is generated about 1 μs after firing the discharge.

An x-ray pinhole camera and x-ray spectrograph were used to study the gas-puff, z-pinch device and provide spectroscopy. Fig. 1 shows schematically the x-ray diagnostic arrangement. X-ray spectra were collected with flat-crystal optics onto Kodak No-Screen x-ray film. The spectrograph was placed in a helium-filled tube and isolated from the vacuum discharge device by a 0.0013 cm Kapton window. Aluminized Kimfol was used to provide a light-tight cover over the x-ray film. The diffraction crystals used to collect x-ray spectra in the 3-8 Å region were LiF (2d = 4.028 Å), Ge (2d = 6.533 Å), and Pentaerythritol (PET, 2d = 8.726 Å). On some shots a 500 μm slit was used to acquire spatially resolved Ar spectra. The x-ray pinhole camera was used to record the plasma image simultaneously with the x-ray spectral data. The pinhole

camera consisted of apertures of sizes 15, 50, and 100 μm diameter in
0.0025 cm Au foil and a film stack. The front film was a Kodak fine-
grain x-ray film while Kodak No-Screen was used as the second film. The
front film recorded all the Ar line radiation while the second film
recorded radiation primarily below about 3.5 Å, including all of the Ar
radiation from transitions with an $n \geq 3$ upper level. The image of the
plasma column formation was recorded with various film combinations and
magnifications for determining the size of the pinch plasma regions.

Spectral intensities were obtained by correcting the measured film
densities. Film densities were recorded every 10 μm across the films
using a 10 or 20 μm wide densitometer slit width. The spectra were
scanned with a digitizing Grant densitometer. The film densities were
converted to spectral intensities using No-Screen sensitometric data,[5]
published x-ray absorption coefficients for the filters,[6] and flat
crystal integral reflection coefficients.[7] X-ray line ratios were
obtained from integrated spectral intensities.

Plasma temperatures were determined from model calculations being
developed at the Naval Research Laboratory.[8] A collisional-radiative
equilibrium transport model (C.R.E.) was used for interpreting the Ar
spectra. The model solves rate equations involving the ground-state
levels and 16 excited-state levels in the H- and He-like ionization
stages. The radiation transport allows for photon escape from optically
thick plasma by frequency diffusion into a broadened line profile. Three
sets of line ratios involving the He- and H-like ionization stages were
calculated at an ion density of 1×10^{20} cm^{-3} corresponding to an electron
density of about 1.6×10^{21} el/cm^3 for finite pinched regions with

between 30 and 250 μm diameters. Plasma temperatures for Al spectra, generated in the gas-puff discharge device by exploding a thin wire, were determined from line ratio calculations for imploded wire plasmas.[9] The plasma temperature for the Kr spectrum was estimated from the abundance of ionization stages using coronal model calculations.[10]

III. Results

A. Plasma Images

Some 40 sets of time-integrated, x-ray pinhole images were collected for the Ar gas puff shots with various size pinholes and films. The images consisted of a collinear pattern of closely spaced or overlapping pinched-plasma spots. Fig. 2 shows the image acquired through a 100 μm pinhole. The collinear series of pinches formed in Ar plasmas is seen to extend from the anode surface to the cut off formed by the cathode structure. An inter-electrode distance of ~ 7 mm is viewed by the pinhole camera. The plasma column forms at the center of the hollow gas jet in the z-pinch device. In only one Ar shot the plasma column was non-collinear, but rather had a short curved tail midway along the column. After achieving the proper operational conditions, principally the amount of gas injection and the delay time between the gas valve and the capacitor discharges, intense pinching was observed on every shot. There is shot-to-shot variation in the position of the pinches along the inter-electrode spacing, but the image in Fig. 2 is typical for Ar shots.

The size and shape of the Ar plasma pinches was determined from pinhole images collected with lower exposure and thru smaller apertures. Depending on the exposure level, lengths up to 4 mm of continuous-looking

plasma were observed. However at low-exposure level individual pinched areas or spots were visible. Fig. 3 shows the Ar plasma images for shot 33. The images were collected on fine grain Kodak Panatomic X film (front) and Kodak No-Screen film (second). The collinear pattern of pinched spots (limited by the 100 μm pinhole) is observed. The outline of the anode is more visible in the second film indicating energetic x-rays with energies above 3-4 keV. On some shots a third film (No Screen) was placed in the stack. The image formed from x-rays with energies > 6 keV was that of the anode structure without pinches. The amount of flaring-like radiation on the anode side of the pinches is barely visible. A 15 μm diameter pinhole in 0.0025 cm Au foil was used to determine the size of the pinches. The pinched areas were found to be between 50 and 100 μm in diameter. Also the size of the plasma column generally varied between 50 and 100 μm.

The pinhole images of Kr plasmas indicated that only a few pinches were formed by the plasma implosion. Fig. 4 shows a typical image. In the Kr shots, the pinches always occurred away from the anode; and a broad plasma column (1/2-1 1/2 mm diameter) was observed between the pinches and the anode. The Kr pinches were again 50-100 μm in size and were visible only on the first film of the stack because of the longer wavelength of the Kr spectral lines. The plasma column emanating from the pinches was more intense on the second film of the stack.

B. Argon

Argon spectra were collected with LiF and Ge crystals from the gas-puff z-pinch device. Fig. 5 shows a spectral region containing the He- and H-like resonance lines in Ar XVII and XVIII for shot 33. The

Li-like k,j satellite lines in Ar XVI are identified, together with radiation from Ar XV. In one shot 1s-2p type transitions were observed for ionization stages down to Ar X. The spin-orbit splitting in the 2p configuration can be seen for the H-like resonance transitions. This indicates a resolving power of 700 for the Ge crystal based on a calculated separation of 5.4 milli angstroms.[11] This spectrum was obtained with spatial resolution from the intense pinch indicated in Fig. 3. The Argon wavelengths used in this work were those published by Peacock for the He-like transitions in Ar XVII.

The Ar plasma electron temperature was determined from two pairs of line ratios calculated for 50 and 100 μm spots in the C.R.E. model. The integrated ratios of the Ar XVIII Lyman alpha lines to both the Ar XVII $1s^2$-1s2p ^{1}P and the $1s^2$-1s3p ^{1}P lines were used. The temperatures estimated from the two sets of lines agreed within 30 eV. The Ar plasma temperature produced in the pinched region in shot 33 was 925-1025 eV. The 100 eV temperature range corresponds to calculations for a 100 μm and 50 μm pinched plasma diameter, with the higher temperature associated with a smaller plasma size. The He-like resonance line ($1s^2$-1s2p ^{1}P) is optically thick for 50-100 μm diameter plasmas at an ion density of 1×10^{20} cm^{-3}. The optical depth varies between 15 and 30. All other transitions generated in the Ar plasma under these conditions and at a plasma temperature of $\sim$ 1 keV have optical depths of less than unity. For the temperature, density, and lifetime determined in this experiment, the pinched Ar plasma is in a state near coronal equilibrium. A plasma temperature estimate based on coronal-equilibrium plasma-model calculations including the effect of dielectronic recombination yields a temperature of 1.0 keV

-53-

for Ar. A recombination temperature of 825 eV was determined from the intense k,j dielectronic satellite lines in Ar XVI based on theoretical work[12] for the Li-like transition satellite to the He-resonance line. These calculations are for low density optically thin plasmas. The assumption is made in this work that the opacity of the ^1P line produces a frequency redistribution of line radiation in the transport from the dense plasma region. This effect would produce line broadening of the ^1P line. The He-like resonance line is observed to be 30% wider than the ^3P intercombination line at half maximum intensity. The integrated line ratio of the He-like resonance ^1P and intercombination ^3P transitions can be used to estimate the density for the pinched plasma. An electron density of 3×10^{21} cm^{-3} was determined based on theoretical calculations for laser-produced plasmas[13] and the ^1P to ^3P line ratio for shot 33.

The higher Rydberg transitions in Ar yielded additional temperature and density diagnostics together with intense satellite spectral lines. The high Rydberg transitions in Ar were recorded after changing the crystal angle in the x-ray spectrograph. Fig. 6 shows an Ar spectrum in the 3-3.5 Å region collected with a LiF crystal. The He-like Rydberg transitions in Ar XVII were observed up to $1s^2$-1s8p in this shot. The series merging technique[14] yields an electron density estimate of 2×10^{21} cm^{-3}. In other shots, the $1s^2$-1s8p line in Ar XVII was also the highest Rydberg transition before merging into the continuum occurred. However on one shot a weak indication of the $1s^2$-1s9p line was present which yields a corresponding density of 8×10^{20} el/cm^3. The plasma temperature was determined from the 3-3.5 Å Ar spectra from the line ratio of the 1s-3p/$1s^2$-1s5p lines. These lines are close in wavelength

-54-

and hence any experimental uncertainty in processing the spectral inten-
sities is minimized. This line ratio gave a plasma temperature of 950-
1050 eV based on the C.R.E. calculations for the spectrum shown in
Fig. 6. On other shots collected with the Ge crystal the spectral lines
were more intense above the background radiation and the hydrogenic
1s-4p line in Ar XVIII was observed. However, the Ar spectra did not
have sufficient intensity to determine a plasma temperature from the
slope of the hydrogenic free-bound continuum. Fig. 6 shows the calcu-
lated line pattern for the Li-like satellites for the He-like Rydberg
transition in Ar from atomic structure calculations.[15] The theoretical
oscillator strengths, gf-values, for each of the transitions are obtained
for the calculated wavelengths in the configurations with 2s and 2p
electrons in the ground state. The calculated wavelengths were normalized
by $+3$ mÅ before plotting. It can be seen that there is agreement between
the calculated and observed satellite structure. Table I gives the
classification of the experimental satellite lines. The most intense
satellite lines arise from ^2D terms in the upper configurations.

Spectral variations were found in Ar spectra collected without
spatial resolution from the plasma implosion regions. In some Ar puff
gas shots, the plasmas had about 100 eV lower temperature than in shots
generating ~ 1 keV plasma. In shot 47 the H- to He-like $1s-2p/1s^2-1s2p$
line ratio gave a plasma temperature 825-925 eV based on the collisional-
radiative equilibrium model for 100 and 50 μm pinched diameters. A
correspondingly lower recombination temperature of 700 eV was found for
the intensity of the k,j lines. The electron density was determined to
be 2×10^{21} cm^{-3}. Another shot (39) for which the high Rydberg transitions

were collected with the Ge crystal had a lower plasma temperature of 800-900 eV based on the $1s-3p/1s^2-1s5p$ line ratio. In Fig. 6 the ^2D satellite has a wavelength of 3.429 Å and coincides with the line identification by Peacock and Cowan[16] as the $1s^2 2p\ ^1P-1s2p3p\ ^2D$ line in Ar XVI. The ratio of this satellite line and the satellite line at 3.275 Å to the $1s^2-1s5p$ line exhibited large shot-to-shot variations. The striking feature of shot 39 was that these two satellite lines were about 75% the intensity of their parent $1s^2-1s3p$ and $1s^2-1s4p$ lines in Ar XVII.

In the gas-puff data, Ar Kα and Kβ lines were not present at a detectable level. X-rays from these lines would be produced by energetic electrons forming inner-shell vacancies in cool-plasma regions. Energetic x-rays (> 3.5 keV) are seen to be emitted from the anode in the pinhole images for Ar plasmas. The slit in front of the spectrograph limited the view to the imploded plasma. The dense plasma in the gas puff pinched to uniform diameters (Fig. 3) with only a small amount of flaring towards the anode. In contrast, the images produced in exploded-single-wire experiments have large cool-plasma flares (anode side of each pinch).[17] Cl Kα x-rays produced by inner-shell ionization in cool plasma were detected in a Cl spectrum in a single exploded-wire experiment using a small diameter strip of saran; but Cl Kα lines were not detectable in spectra produced by plasma implosion from an exploded array of multiple saran strips.[18] Both the absence of inner-shell radiation and the images of the pinched regions in the gas-puff data indicate similarities in plasma formation between the z-pinches in the gas puff and plasma implosions from circular arrays of exploded wires.

-56-

C. Krypton

Kr spectra were collected with a PET crystal from the gas-puff z-pinch device. Figs. 7 and 8 show Kr spectra with 2-3 level transitions in the 6.2-7.6 Å region. The dominant lines are identified as Ne-like Kr XXVII. The F-like transitions in Kr XXVIII were observed to be similar to laser-produced spectral patterns found in Zn, Ge, and Se.[19] Lines on the long wavelength side of the 2p-3s and 2p-3d Ne-like transitions in Kr XXVII are satellite lines associated primarily with the Na-like Kr XXVI ionization stage.

The Kr spectral wavelengths were calibrated with the H- and He-like lines from Al plasmas, and the spectra lines were classified using relativistically-corrected Hartree-Fock calculations.[20] Table II gives the experimental wavelengths and relative intensities for the Kr XXVII lines. The wavelengths determined for Kr agreed within 2 mÅ with values interpolated from laser data for the L-series x-rays studies for elements Zn (30) thru Mo (42) at the Naval Research Laboratories[21] and at the Lebedev Physics Institute.[22] The calculated line pattern for the 2p-3s transitions (plotted without normalization) in Na-like Kr XXVI and F-like Kr XXVIII agree reasonably well with the observed spectrum in Fig. 7. The satellite lines in Kr XXVI are classified in Table III. In Fig. 8 the 2p-3s satellite lines between 6.7 and 7.0 Å are complex and calculations were not performed for Kr. The spectral pattern in Kr is similar to those produced in exploded-Mo-wire plasmas for which the Na- and Mg-like transitions have been identified.[23] The most intense satellite transitions were identified as belonging to transitions in Na-like Mo XXXII configurations with a 3s, 3p, or 3d electron in the lower

-57-

configuration. The F-like transitions are distinct in the Kr spectrum, and the calculations for the 2p-3s and 2p-3d transitions in Kr XXVIII are shown in Figs. 7 and 8, respectively. Classifications for the F-like lines are presented in Table IV. Isoelectronic extrapolation of the 2p-3s F-like transitions, previously measured in Zn, Ge, and Se, are in good agreement with the present determinations in Kr listed in the table, except for the 7.209 Å line. From the observed distribution of ionization stages identified in the Kr spectrum, a Kr plasma temperature of 1.5 keV is obtained from the coronal model.

D. Aluminum

Highly-ionized Al spectra were acquired primarily for wavelength calibration of the Kr lines in the 6-7.6 Å region. However, the production of the Al spectra by exploded wire is interesting in demonstrating that high temperature plasmas can by produced by exploding wires in a small-scale discharge generator. Al spectra were produced from explosion of 0.0015 cm wires stretched between the anode and cathode in this long-pulse generator. The electrical discharge characteristics were not optimized for the exploding wires, but the Al spectra provided excellent calibration lines for the Kr data. The Kr wavelengths could be measured to a precision of ± 0.003 Å by reading the spectral films on a Grant comparator densitometer. The only spectral data used were from shots in which the pinhole images of the plasma showed that collinear pinches were formed by the imploded gas and the exploded wire.

Spectra produced with puffed-Ar-gas and Al wires provided useful Al spectral results. Fig. 9 shows the H- and He-like resonance lines. The satellite structure for this spectral region has been identified in

-58-

for laser-produced Al-spectra.[24] The He-like lines satellite to the 1s-2p Lyman alpha transition in Al XIII have also been studied at the Lebedev Physical Institute.[25] The intense satellite line at 7.275 Å is identified as the $1s2p\ ^1P_1 - 2p^2\ ^1D_2$ transition in Al XII in agreement with these earlier reports. The relative line ratio of the hydrogen to helium-like resonance lines gave a plasma temperature of 400 eV based on the C.R.E. model. The electron density from the ratio of resonance and intercombination lines was 2×10^{20} cm^{-3}. The high Rydberg transitions in Al were recorded with the PET crystal and are shown in Fig. 10. The $1s^2$-1s9p line was the last series transition observed yielding a plasma electron density of 3×10^{20} cm^{-3}. The measured 1s-3p/$1s^2$-1s5p line ratio gave a plasma temperature of 450 eV (thin plasma calculation). The transitions satellite to the $1s^2$-1s3p and $1s^2$-1s4p He-like transitions have been identified with the aid of atomic structure calculations in Fig. 10. The most intense satellite at 6.805 Å is identified as the $1s^2 2p$ $^2P - 1s2p(^3P)3p\ ^2D$ transition in Al XI in agreement with previous classifications for laser-produced spectra.[24] The spectral peak adjacent to the $1s^2$-1s3p peak in the short wavelength side is undetermined. Classifications in the Al XI spectrum are given in Table V.

IV. SUMMARY

The collection of x-ray spectral data and pinhole images has provided insight into the z-pinched plasma formed in the gas-puff z-pinch device. This device produces hot plasma pinches in every shot. The Ar images showed a collinear column of pinched-plasma regions with sizes between 50 and 100 μm in diameter. The pinches have electron densities

of $\sim 2 \times 10^{21}$ cm^{-3} and plasma temperatures between 925 and 1050 eV determined from line ratio calculations. In a few Ar shots, the plasma was formed with temperatures about 100 eV lower. The Ar spectra generated by the gas-puff z-pinch device are similar to Ar spectra produced by the dense-plasma-focus device. Some shots produced enhanced ^{2}D satellite lines in Li-like Ar XVI. Inner shell K radiation was not detectable from plasma formed in the inter-electrode gap.

The value of this source for spectroscopy of highly-ionized atoms is demonstrated by analysis of Kr x-ray spectra. The gas puff shots with Kr formed a few pinches midway in the inter-electrode spacing. These pinches have plasma temperatures of about 1.5 keV, and emit intense Ne-like Kr XXVII lines. The 2p-3s spectral lines in Na-like Kr XXVI and the 2p-3s, 2p-3d, and 2s-3p transitions in F-like Kr XXVIII have been measured and classified with atomic structure calculations. The agreement between the wavelengths measured in this work and both calculated and isoelectronically extrapolated wavelengths was within 7 mÅ for most all of the transitions reported. The accuracy in the experimental wavelength determinations in Kr is therefore 0.1%.

The discharge device was capable of exploding thin Al wires to produce high density pinches with 450 eV plasma temperatures and electron densities of $\sim 3 \times 10^{20}$ cm^{-3}.

REFERENCES

1. J. Shiloh, A. Fisher, and N. Rostoker, Phys. Rev. Lett. 40, 515 (1978); J. Shiloh, Ph.D Thesis, University of Calif., Irvine, June 78 (unpublished).

2. N. J. Peacock, R. J. Speer, and M. G. Hobby, J. Phys. B. 2, 798 (1969).

3. D. J. Nagel, C. M. Dozier, B. M. Klein, J. W. Mather, Bull. Am. Phys. Soc. 18, 1363 (1973) (unpublished).

4. A. Fisher, F. Mako, and J. Shiloh, Rev. Sci. Instr. 49, 872 (1978).

5. C. M. Dozier, D. B. Brown, L. S. Birks, P. B. Lyons, and R. F. Benjamin, J. Appl. Phys. 47, 3732 (1976).

6. Burton L. Henke and Eric S. Ekisu, Adv. X-Ray Analysis 13, 639 (1969).

7. J. V. Gilfrich, D. B. Brown, and P. G. Burkhalter, Appl. Spectros. 29, 322 (1975).

8. D. Duston, J. Davis, and K. G. Whitney (unpublished).

9. P. G. Burkhalter, J. Davis, J. Rauch, W. Clark, G. Dahlbacka, and R. Schneider, J. Appl. Phys. 49, xxxx (1978).

10. C. Breton, C. De Michelis, M. Finkenthal, M. Mattioli, Ionization Equilibrium of Selected Elements from Neon to Tungsten of Interest in Tokamak Plasma Research, EUR-CEA-FC-948, Mar. 1978 (unpublished).

11. J. D. Garcia and J. E. Mack, J. Opt. Soc. Am. 55, 654 (1965).

12. C. P. Bhalla, A. H. Gabriel, and L. P. Presnyakov, Mon. Not. R. astr. Soc. 172, 359 (1975).

13. A. V. Vinogradov, I. Yu. Skobelev, and E. A. Yukov,
Sov. J. Quant. Electron. $\underline{5}$, 630 (1975).

14. J. Davis, "Series Merging Technique," N.R.L. Memorandum
Report 2655, Oct. 1973 (unpublished).

15. R. D. Cowan, J. Opt. Soc. Am. $\underline{58}$, 808 (1968).

16. N. J. Peacock and R. D. Cowan, Hartree-Fock calculations
presented in Ref. 2.

17. P. G. Burkhalter, C. M. Dozier, and D. J. Nagel, Phys.
Rev. A$\underline{15}$, 700 (1977).

18. P. G. Burkhalter and R. Schneider (unpublished).

19. P. G. Burkhalter, G. A. Doschek, U. Feldman, Robert D.
Cowan, J. Opt. Soc. $\underline{67}$, 741 (1977).

20. R. D. Cowan and D. C. Griffin, J. Opt. Soc. Am. $\underline{66}$, 1010
(1976).

21. P. G. Burkhalter, D. J. Nagel, and Robert D. Cowan, Phys.
Rev. A$\underline{11}$, 782 (1975).

22. E. V. Aglitskii, V. A. Boiko, O. N. Krokhin, S. A. Pikuz,
and A. Ya. Faenov, Sov. J. Quant. Electron. $\underline{4}$, 1152 (1975).

23. P. G. Burkhalter, R. Schneider, C. M. Dozier, and Robert
D. Cowan, Phys. Rev. A$\underline{17}$,   (1978).

24. U. Feldman, G. A. Doschek, D. J. Nagel, R. D. Cowan, and
R. R. Whitlock, Astrophs. J. $\underline{192}$, 213 (1974).

25. V. A. Boiko, A. Ya. Faenov, S. A. Pikuz, and U. I.
Safronova, Mon. Not. R. astr. Soc., $\underline{181}$, 107 (1977).

Table I. Experimental and calculated Li-like satellite transitions in Ar XVI.

Expt. wavelength λ (Å)	Calc. λ (Å)	gf	J^a	J'^a	E'^a (cm^{-1})	Classification	Composition of upper level (LS-coupling)
3.429 {	3.426	0.26	3/2	5/2	29 194 000	$1s^2 2p - 1s2p3p$	0.92 $1s2p(^3P)3p$ ^2D
	3.426	0.13	1/2	3/2	29 172 000	"	0.82 $1s2p(^3P)3p$ ^2D
3.42 sh {	3.416	0.14	1/2	3/2	29 270 000	$1s^2 2s - 1s2s3p$	0.98 $1s2s(^3S)3s$ ^2P
	3.416	0.07	1/2	1/2	29 272 000	"	0.99 $1s2s(^3S)3p$ ^2P
3.406	3.402	0.06	1/2	3/2	29 393 000	$1s^2 2s - 1s2s3p$	1.00 $1s2s(^1S)3p$ ^2P
3.275 }	3.271	0.06	3/2	3/2	30 582 000	$1s^2 2p - 1s2p4p$	0.43 $1s2p(^3P)4p$ ^2P
	3.270	0.08	3/2	5/2	30 593 000	"	0.91 $1s2p(^3P)4p$ ^2D
	3.270	0.05	1/2	3/2	30 567 000	"	0.51 $1s2p(^3P)4p$ ^2D
3.266 {	3.259	0.05	1/2	3/2	30 683 000	$1s^2 2s - 1s2s4p$	0.98 $1s2s(^3S)4p$ ^2P
	3.259	0.03	1/2	1/2	30 684 000	"	1.00 $1s2s(^3S)4p$ ^2P
3.250	3.245	0.02	1/2	3/2	30 819 000	$1s^2 2s - 1s2s4p$	1.00 $1s2s(^3S)4p$ ^4P
3.203[b] {	3.202	0.03	3/2	5/2	31 237 000	$1s^2 2p - 1s2p5p$	0.86 $1s2p(^3P)5p$ ^2D
	3.202	0.02	1/2	3/2	31 213 000	"	0.65 $1s2p(^3P)5p$ ^2D
3.194 {	3.192	0.03	1/2	3/2	31 332 000	$1s^2 2s - 1s2s5p$	0.98 $1s2s(^3S)5p$ ^2P
	3.192	0.01	1/2	1/2	31 332 000	"	1.00 $1s2s(^3S)5p$ ^2P

Table I. Experimental and calculated Li-like satellite transitions in Ar XVI, continued.

Expt. wavelength (Å)	Calc. λ (Å)	gf	J^a	J'^a	E'^a (cm^{-1})	Classification	Composition of upper level (LS-coupling)
3.166	3.167	0.01	3/2	3/2	31 583 000	$1s^2 2p$-$1s2p6p$	0.59 $1s2p(^3P)6p$ ^2P
	3.167	0.02	3/2	5/2	31 586 000	"	0.83 $1s2p(^3P)6p$ ^2D
	3.167	0.01	1/2	3/2	31 562 000	"	0.64 $1s2p(^3P)6p$ ^2D
3.156^c	3.156	0.02	1/2	3/2	31 682 000	$1s^2 2s$-$1s2s6p$	0.98 $1s2s(^3S)6p$ ^2P
	3.156	0.01	1/2	1/2	31 683 000	"	1.00 $1s2s(^3S)6p$ ^2P
3.145	3.146	0.01	3/2	3/2	31 794 000	$1s^2 2p$-$1s2p7p$	0.60 $1s2p(^3P)7p$ ^2P
	3.146	0.01	3/2	5/2	31 796 000	"	0.81 $1s2p(^3P)4p$ ^2D

a) The symbols J and J' represent the total angular momentum of the lower and upper levels, respectively. The symbol E' is the theoretical eigenvalue of the upper configuration.

b) Wavelength of the $1s^2$-$1s4p$ transition is 3.203 A.

c) Wavelength of the 1s-3p line in Ar XVIII is 3.156 A.

sh = shoulder

Table II. Experimental values for Ne-like transitions in Kr XXVII.

Expt. wavelength (Å)	Expt. Int.	Interp. λ (Å)	Classification in (j-j) coupling
7.507	80	7.506	$2p^6-2p^5(^2P_{3/2}),3s$
7.269	55	7.271	$2p^6-2p^5(^2P_{1/2}),3s$
6.958	60	6.959	$2p^6-2p^5(^2P_{3/2}),3d(^2D_{3/2})$
6.881	100	6.883	$2p^6-2p^5(^2P_{3/2}),3d(^2D_{5/2})$
6.699	95	6.701	$2p^6-2p^5(^2P_{1/2}),3d(^2D_{3/2})$
6.385	35	6.387	$2s^2\,2p^6-2s2p^6\,3p(^2P_{1/2})$
6.336	45	6.338	$2s^2\,2p^6-2s2p^6\,3p(^2P_{3/2})$

Table III. Experimental and calculated Na-like satellite transitions in Kr XXVI.

Expt. wavelength (Å)	Calc. λ (Å)	gf	J^a	J'^a	E'^a (cm^{-1})	Classification	Composition of upper level[b] (j-j coupling)
7.634	7.631	0.06	3/2	3/2	13 138 000	$2p^6 3p-2p^5 3s3p$	$0.70(^2P_{3/2}, {}^2S_{1/2}, {}^2P_{3/2})$
7.623 {	7.626	0.06	3/2	5/2	13 146 000	$2p^6 3p-2p^5 3s3p$	$0.58(^2P_{3/2}, {}^2S_{1/2}, {}^2P_{3/2})$
	7.623	0.08	1/2	3/2	13 052 000	$2p^6 3p-2p^5 3s3p$	$0.86(^2P_{3/2}, {}^2S_{1/2}, {}^2P_{1/2})$
7.614 }	7.614	0.08	3/2	5/2	13 120 000	$2p^6 3d-2p^5 3s3d$	$0.60(^2P_{3/2}, {}^2S_{1/2}, {}^2D_{3/2})$
	7.612	0.04	1/2	1/2	13 071 000	$2p^6 3p-2p^5 3s3p$	$0.91(^2P_{3/2}, {}^2S_{1/2}, {}^2P_{1/2})$
	7.610	0.11	5/2	5/2	13 149 000	$2p^6 3d-2p^5 3s3d$	$0.47(^2P_{3/2}, {}^2S_{1/2}, {}^2D_{5/2})$
7.604 {	7.607	0.07	5/2	7/2	13 155 000	$2p^6 3d-2p^5 3s3d$	$0.62(^2P_{3/2}, {}^2S_{1/2}, {}^2D_{5/2})$
	7.605	0.11	3/2	3/2	13 135 000	$2p^6 3d-2p^5 3s3d$	$0.76(^2P_{3/2}, {}^2S_{1/2}, {}^2D_{3/2})$
7.594 }	7.599	0.07	5/2	3/2	13 168 000	$2p^6 3d-2p^5 3s3d$	$0.65(^2P_{3/2}, {}^2S_{1/2}, {}^2D_{5/2})$
	7.597	0.04	3/2	5/2	13 149 000	$2p^6 3d-2p^5 3s3d$	$0.47(^2P_{3/2}, {}^2S_{1/2}, {}^2D_{5/2})$
	7.594	0.08	5/2	7/2	13 177 000	$2p^6 3d-2p^5 3s3d$	$0.48(^2P_{3/2}, {}^2S_{1/2}, {}^2D_{5/2})$
7.570 {	7.576	0.06	5/2	5/2	13 208 000	$2p^6 3d-2p^5 3s3d$	$0.43(^2P_{3/2}, {}^2S_{1/2}, {}^2D_{5/2})$
	7.573	0.08	1/2	3/2	13 204 000	$2p^6 3s-2p^5 3s^2$	$1.0(^2P_{3/2}, {}^1S_0)$

Table III. Experimental and calculated Na-like satellite transitions in Kr XXVI, continued

Expt. wavelength λ (Å)	Calc. λ (Å)	gf	J^a	J'^a	E'^a (cm^{-1})	Classification	Composition of upper level[b] (j-j coupling)
7.554	7.557	0.07	3/2	5/2	13 267 000	$2p^63p-2p^53s3p$	$0.49(^2P_{3/2}, {}^2S_{1/2}, {}^2P_{3/2})$
7.538							
7.393	7.393	0.09	3/2	5/2	13 560 000	$2p^63p-2p^53s3p$	$1.0(^2P_{1/2}, {}^2S_{1/2}, {}^2P_{3/2})$
7.384	{ 7.386	0.05	1/2	3/2	13 473 000	$2p^63p-2p^53s3p$	$0.86(^2P_{1/2}, {}^2S_{1/2}, {}^2P_{1/2})$
	7.384	0.04	5/2	5/2	13 551 000	$2p^63d-2p^53s3d$	$0.49(^2P_{1/2}, {}^2S_{1/2}, {}^2D_{5/2})$
7.376	{ 7.379	0.06	3/2	5/2	13 539 000	$2p^63d-2p^53s3d$	$0.74(^2P_{1/2}, {}^2S_{1/2}, {}^2D_{3/2})$
	7.376	0.11	5/2	7/2	13 566 000	$2p^63d-2p^53s3d$	$1.0(^2P_{1/2}, {}^2S_{1/2}, {}^2D_{5/2})$
	7.368	0.05	5/2	3/2	13 581 000	$2p^63d-2p^53s3d$	$0.81(^2P_{1/2}, {}^2S_{1/2}, {}^2D_{5/2})$
7.350	7.351	0.05	5/2	5/2	13 612 000	$2p^63d-2p^53s3d$	$0.53(^2P_{1/2}, {}^2S_{1/2}, {}^2D_{5/2})$
7.322	7.338	0.03	1/2	1/2	13 628 000	$2p^63s-2p^53s^2$	$1.0(^2P_{1/2}, {}^1S_0)$

a) The symbols J and J′ represent the total angular momentum of the lower and upper levels, respectively. The symbol E′ is the theoretical eigenvalue of the upper configuration.

b) The square of the largest eigenvector component is listed.

TABLE IV. Experimental and calculated values for F-like transitions in Kr XXVIII.

Expt. wavelength (Å)	Extrap. λ (Å)	Calc. λ (Å)	gf	J^a	J'^a	E'^a (cm^{-1})	Transition and composition of upper level[b,c]	
							(j-j coupling)	(LS coupling)
						2p^5–2p^{4}3s		
7.209	7.200	7.206	0.04	3/2	5/2	13 728 000	0.78($^3P_2$,1/2)	0.78(^{3}P)$^4P_{5/2}$
		7.202	0.07	1/2	1/2	14 187 000	0.99($^3P_2$,1/2)	0.68(^{3}P)$^2P_{1/2}$
7.193	7.189	7.188	0.22	3/2	3/2	13 761 000	0.75($^3P_2$,1/2)	0.60(^{3}P)$^2P_{3/2}$
7.162	7.168	7.158	0.14	1/2	3/2	14 271 000	0.75($^1D_2$,1/2)	0.75(^{1}D)$^2D_{3/2}$
7.123		7.120	0.05	3/2	1/2	13 895 000	0.51($^3P_2$,1/2)	0.48(^{1}S)$^2S_{1/2}$
6.997	6.998	6.988	0.05	3/2	3/2	14 159 000	0.99($^3P_2$,1/2)	0.83(^{3}P)$^4P_{3/2}$
6.975	6.978	6.975	0.04	3/2	1/2	14 187 000	0.99($^3P_2$,1/2)	0.68(^{3}P)$^2P_{1/2}$
6.941	6.942	6.939	0.16	3/2	5/2	14 260 000	0.78($^1D_2$,1/2)	0.78(^{1}D)$^2D_{5/2}$
		6.911	0.07	1/2	1/2	14 771 000	0.51($^1S_2$,1/2)	0.51(^{1}S)$^2S_{1/2}$
						2p^5–2p^{4}3d		
6.881		6.880	0.01	1/2	3/2	14 836 000	0.57($^3P_2$,5/2)	0.33(^{3}P)$^4P_{3/2}$
6.727		6.728	0.01	1/2	3/2	15 164 000	0.72($^3P_0$,3/2)	0.39(^{3}P)$^4D_{3/2}$

Table IV. Experimental and calculated values for F-like transitions in Kr XXVIII (continued)

Expt. wavelength (Å)	Calc. λ (Å)	gf	J^a	J'^a	E'^a (cm^{-1})	Transition and composition of upper level[b,c] (j-j coupling)	(LS coupling)
6.715sh	6.719	0.02	3/2	1/2	14 734 000	$0.61(^3P_2, 3/2)$	$0.33(^3P)^4P_{1/2}$
6.699	6.700	0.19	1/2	3/2	15 226 000	$0.60(^3P_1, 5/2)$	$0.39(^3P)^2P_{3/2}$
6.678	6.688	0.37	3/2	1/2	14 801 000	$0.57(^3P_2, 5/2)$	$0.39(^3P)^4P_{1/2}$
	6.673	0.83	3/2	3/2	14 836 000	$0.57(^3P_2, 5/2)$	$0.33(^3P)^4P_{3/2}$
6.663	6.662	1.72	3/2	5/2	14 861 000	$0.68(^3P_2, 5/2)$	$0.29(^3P)^2D_{5/2}$
	6.660	0.28	1/2	3/2	15 316 000	$0.37(^1D_1, 3/2)$	$0.58(^1D)^2P_{3/2}$
6.639	6.639	0.58	3/2	3/2	14 913 000	$0.30(^1D_1, 5/2)$	$0.38(^3P)^4F_{3/2}$
6.626	6.627	2.09	1/2	3/2	15 391 000	$0.41(^1S_0, 3/2)$	$0.56(^1D)^2D_{3/2}$
	6.624	1.16	3/2	5/2	14 946 000	$0.47(^3P_0, 5/2)$	$0.43(^1S)^2D_{5/2}$
6.614sh	6.617	1.48	1/2	1/2	15 413 000	$0.51(^1D_1, 5/2)$	$0.53(^1D)^2P_{1/2}$
6.519	6.514	0.80	3/2	5/2	15 200 000	$0.66(^3P_1, 3/2)$	$0.49(^3P)^4F_{5/2}$
6.502	6.508	0.21	3/2	5/2	15 214 000	$0.81(^3P_1, 5/2)$	$0.58(^3P)^2F_{5/2}$
6.479	6.476	0.81	3/2	1/2	15 292 000	$0.60(^1D_1, 3/2)$	$0.66(^1D)^2S_{1/2}$
	6.465	1.80	3/2	3/2	15 316 000	$0.37(^1D_1, 3/2)$	$0.58(^1D)^2P_{3/2}$
6.465	6.462	2.82	3/2	5/2	15 325 000	$0.63(^1D_2, 3/2)$	$0.44(^1D)^2F_{5/2}$

Table IV. Experimental and calculated values for F-like transitions in Kr XXVIII (continued)

Expt. wavelength (Å)	Calc. λ (Å)	gf	J^a	J'^a	E^a (cm^{-1})	Transition and composition of upper level[b,c] (j-j coupling)	(LS coupling)
6.449	6.442	1.80	1/2	3/2	15 824 000	$0.49(^3P_0,3/2)$	$0.49(^1S)\,^2D_{3/2}$
6.428	6.434	0.44	3/2	3/2	15 391 000	$0.30(^1D,5/2)$	$0.56(^1D)\,^2D_{3/2}$
6.418	6.425	0.19	3/2	1/2	15 413 000	$0.51(^1D,5/2)$	$0.53(^1D)\,^2P_{1/2}$
					$2s^2 2p^5 - 2s 2p^5 3p$		
6.428	6.428	0.01	1/2	1/2	15 858 000	$0.68(^2S_{1/2},3/2,1/2)$	$0.66(^1P)\,^2S_{1/2}$
	6.302	0.01	1/2	3/2	16 168 000	$0.47(^2S_{1/2},3/2,3/2)$	$0.39(^3P)\,^2P_{3/2}$
6.259	6.247	0.23	3/2	1/2	15 858 000	$0.68(^2S_{1/2},3/2,1/2)$	$0.66(^1P)\,^2S_{1/2}$
6.227	6.227	0.16	3/2	5/2	15 908 000	$0.89(^2S_{1/2},3/2,1/2)$	$0.59(^{3,4}P)\,^4D_{5/2}$
6.214	6.216	0.10	1/2	3/2	16 388 000	$0.88(^2S_{1/2},1/2,1/2)$	$0.43(^3P)\,^4D_{3/2}$
	6.173	0.03	1/2	3/2	16 500 000	$0.66(^2S_{1/2},1/2,3/2)$	$0.54(^3P)\,^4P_{3/2}$
6.171	6.173	0.02	3/2	1/2	16 049 000	$0.45(^2S_{1/2},3/2,3/2)$	$0.38(^1P)\,^2P_{1/2}$
	6.170	0.06	3/2	3/2	16 056 000	$0.49(^2S_{1/2},3/2,3/2)$	$0.26(^3P)\,^4P_{3/2}$
6.166	6.169	0.88	3/2	5/2	16 059 000	$0.88(^2S_{1/2},3/2,3/2)$	$0.60(^1P)\,^2D_{5/2}$
	6.157	0.25	3/2	5/2	16 092 000	$0.98(^2S_{1/2},3/2,3/2)$	$0.59(^3P)\,^4P_{5/2}$
	6.151	0.71	1/2	3/2	16 558 000	$0.69(^2S_{1/2},1/2,3/2)$	$0.53(^3P)\,^2D_{3/2}$

Table IV. Experimental and calculated values for F-like transitions in Kr XXVIII (continued)

Expt. wavelength (Å)	Calc. λ (Å)	gf	J^a	J'^a	E'^a (cm^{-1})	Transition and composition of upper level[b,c]	
						(j-j coupling)	(LS coupling)
6.145	6.140	0.15	3/2	1/2	16 136 000	$0.69(^2S_{1/2},3/2,3/2)$	$0.60(^3P)\,^2S_{1/2}$
	6.140	0.39	1/2	1/2	16 588 000	$0.79(^2S_{1/2},1/2,3/2)$	$0.59(^3P)\,^2P_{1/2}$
6.129	6.128	0.76	3/2	3/2	16 168 000	$0.47(^2S_{1/2},3/2,3/2)$	$0.39(^3P)\,^2P_{3/2}$
					$2s2p^6-2p^6\,3p$		
6.185	6.191	0.21	1/2	1/2	17 896 000	$1.0(^1S_0,1/2)$	$1.0(^2P)\,^2P_{1/2}$
6.145	6.147	0.42	1/2	3/2	18 011 000	$1.0(^1S_0,3/2)$	$1.0(^2P)\,^2P_{3/2}$

a) The symbols J and J´ represent the total angular momentum of the lower and upper levels, respectively. The symbol E´ is the theoretical eigenvalue of the upper configuration.

b) The square of the largest eigenvector component is listed.

c) Abbreviated notation ($^3P_2$,1/2) in place of ($2p^4\ ^3P_2,3s_{1/2}$) in the j-j coupling scheme.

Table V. Experimental and calculated Li-like satellite transitions in Al XI.

Expt. wavelength (Å)	Calc. λ (Å)	gf	J^a	J'^a	E^a (cm^{-1})	Classification	Composition of upper level (LS-coupling)
6.824	6.824	0.05	3/2	3/2	14 657 000	$1s^2 2p-1s2p3p$	0.58 $1s2p(^3P)3p\ ^2P$
6.805	6.805	0.26	3/2	5/2	14 696 000	=	0.93 $1s2p(^3P)3p\ ^2D$
	6.805	0.15	1/2	3/2	14 690 000	=	0.90 $1s2p(^3P)3p\ ^2D$
6.794	6.798	0.06	3/2	1/2	14 711 000	=	0.80 $1s2p(^3P)3p\ ^2S$
6.781	6.780	0.08	3/2	3/2	14 751 000	=	0.92 $1s2p(^1P)3p\ ^2P$
	6.779	0.13	1/2	3/2	14 751 000	$1s^2 2s-1s2s3p$	1.0 $1s2s(^3S)3p\ ^2P$
	6.779	0.07	1/2	1/2	14 752 000	=	1.0 $1s2s(^3S)3p\ ^2P$
6.749	6.740	0.03	1/2	1/2	14 836 000	=	1.0 $1s2s(^2S)3p\ ^2P$
	6.739	0.05	1/2	3/2	14 838 000	=	1.0 $1s2s(^1S)3p\ ^2P$
6.686	6.679	0.16	1/2	3/2	14 973 000	$1s^2 3s-1s3s3p$	0.67 $1s3s(^1S)3p\ ^2P$
	6.679	0.17	3/2	3/2	14 973 000	$1s^2 3p-1s3p^2$	0.58 $1s3p^2(^2D)$
	6.660	0.04	1/2	3/2	15 016 000	$1s^2 3s-1s3s3p$	0.67 $1s3s(^3S)3p\ ^2P$
6.514	6.512	0.02	3/2	3/2	15 359 000	$1s^2 2p-1s2p4p$	0.92 $1s2p(^3P)4p\ ^2D$
	6.510	0.08	3/2	5/2	15 364 000	=	0.98 $1s2p(^3P)4p\ ^2D$
	6.509	0.04	1/2	3/2	15 359 000	=	0.92 $1s2p(^3P)4p\ ^2D$

Table V. Experimental and calculated Li-like satellite transitions in Al XI, continued.

Expt. wavelength (Å)	Calc. λ (Å)	gf	J^a	J'^a	E'^a (cm^{-1})	Classification	Composition of upper level (LS-coupling)
6.488 {	6.485	0.02	3/2	5/2	15 423 000	$1s^2 2p - 1s2p4p$	1.0 $1s2p(^1P)4p\ ^2D$
	6.484	0.02	3/2	3/2	15 425 000	"	0.97 $1s2p(^1P)4p\ ^2P$
	6.482	0.05	1/2	3/2	15 428 000	$1s^2 2s - 1s2s4p$	1.0 $1s2s(^3S)4p\ ^2P$
6.447	6.442	0.03	1/2	3/2	15 524 000	"	1.0 $1s2s(^1S)4p\ ^2P$
6.386	6.376	0.10	3/2	5/2	15 686 000	$1s^2 3p - 1s3p4p$	0.72 $1s3p(^3P)4p\ ^2D$
	6.369	0.07	1/2	3/2	15 701 000	$1s^2 3s - 1s3s4p$	1.0 $1s2s(^3S)4p\ ^2P$
6.360	6.361	0.03	1/2	3/2	15 721 000	"	1.0 $1s2s(^1S)4p\ ^2P$

[a]The square of the largest eigenvector component is listed.
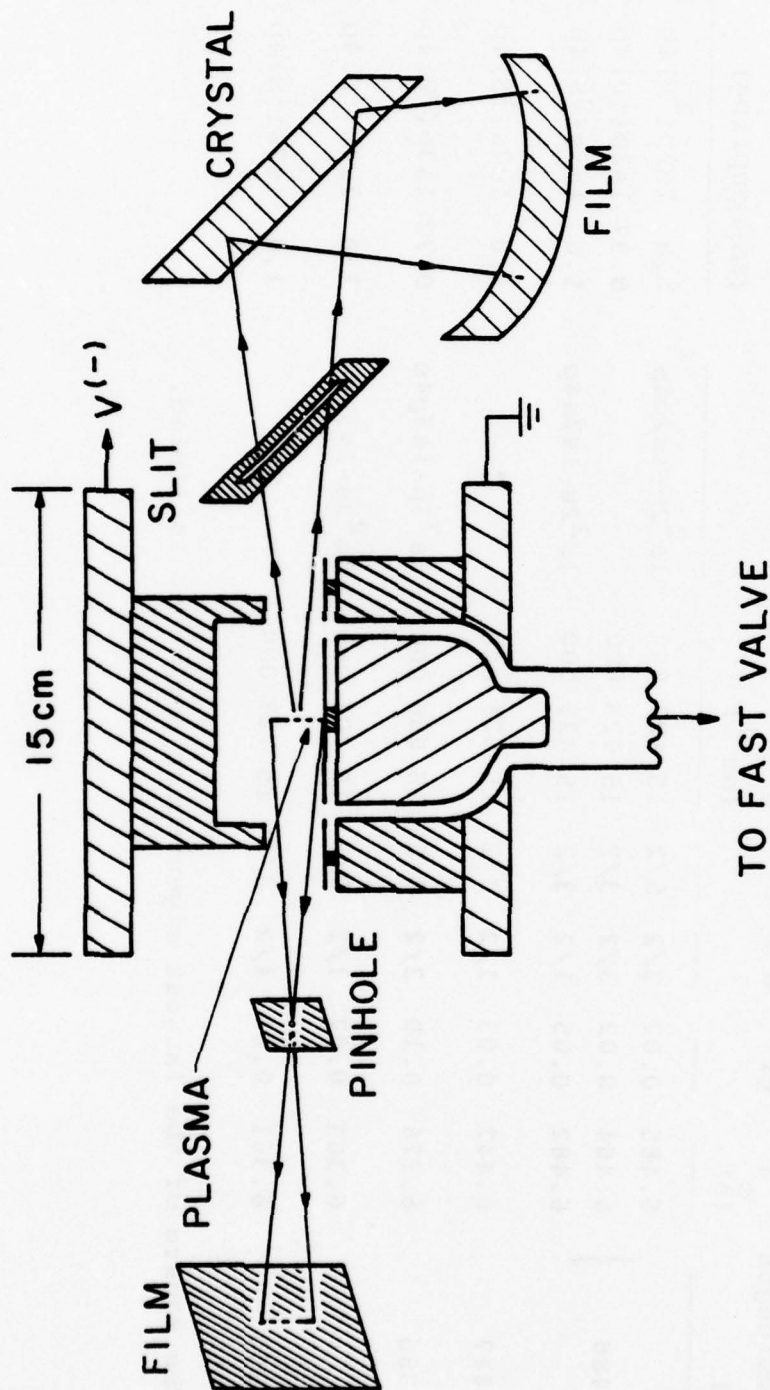
Fig. 1 - Schematic of the x-ray crystal spectrograph and pinhole camera geometry used in the gas-puff, z-pinch device.
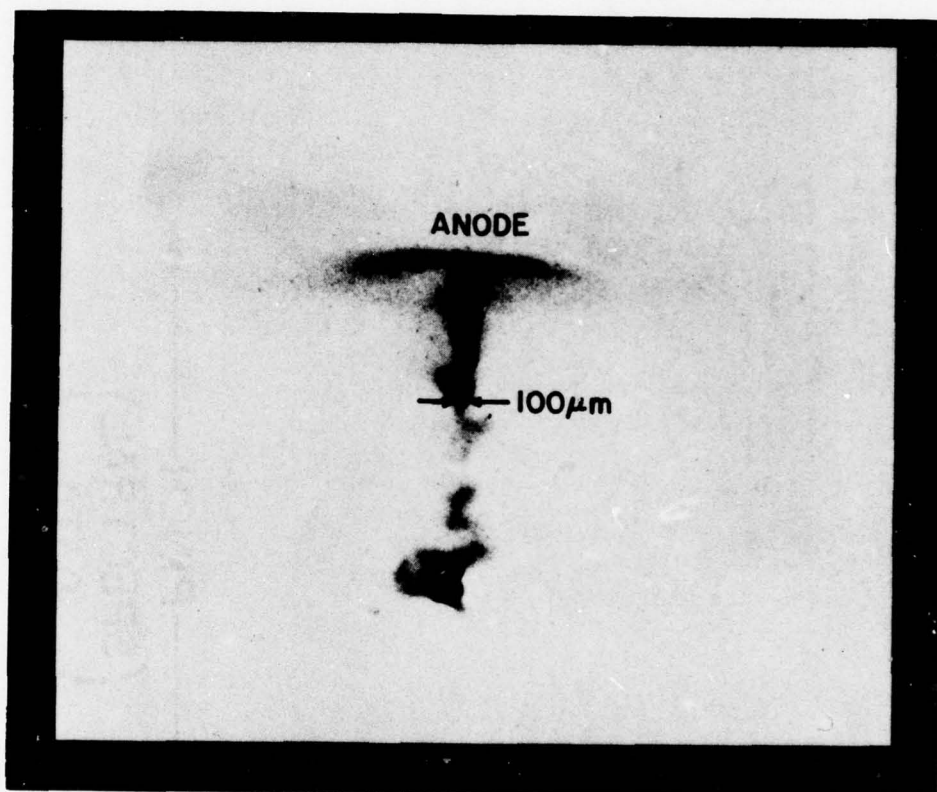
Fig. 2 - Pinhole image of imploded Ar gas puff plasma.
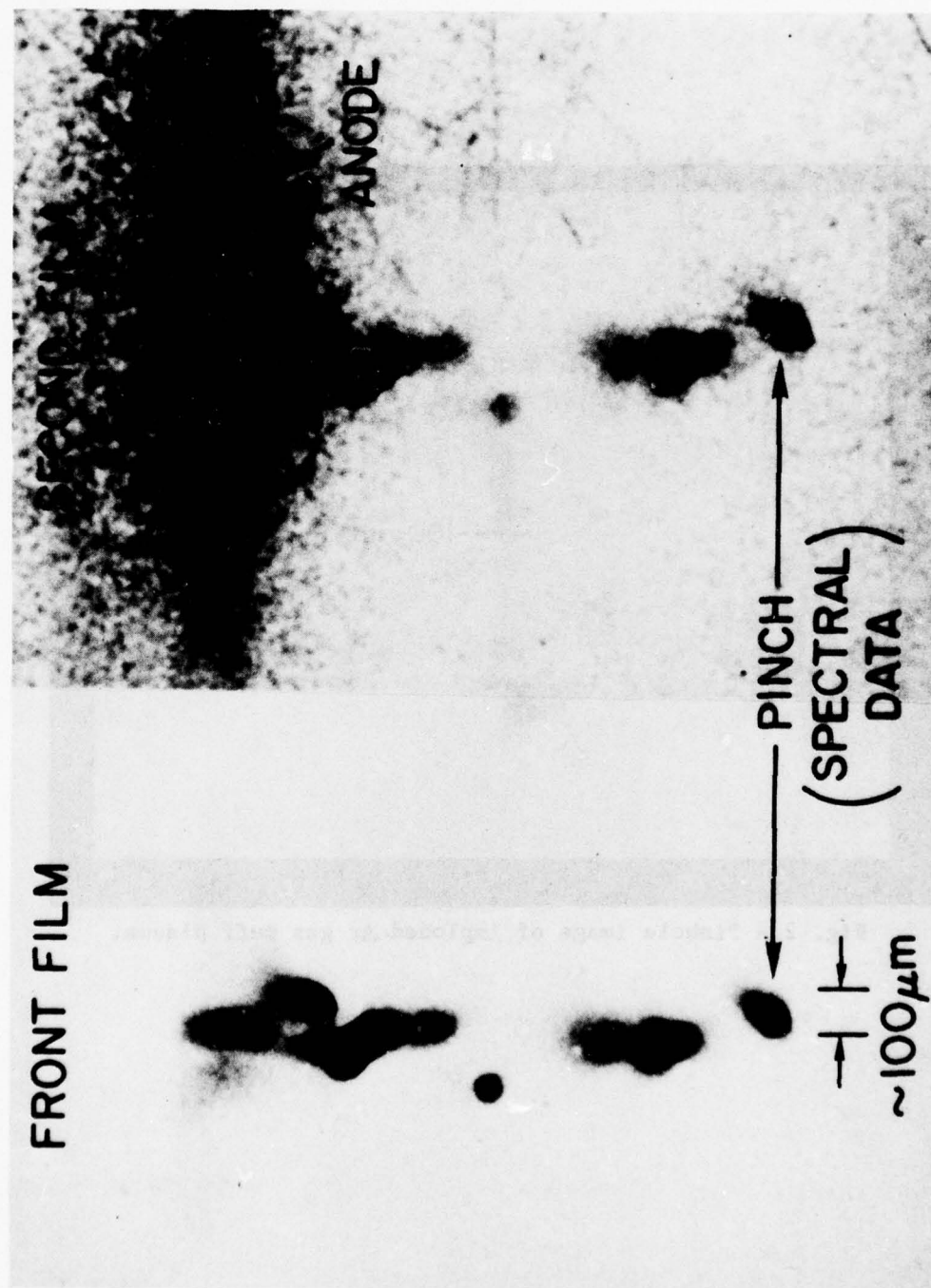
Fig. 3 - Pinhole image of Ar pinched-plasma regions. The front film was Kodak Panatomic X and the second film was Kodak No-Screen.
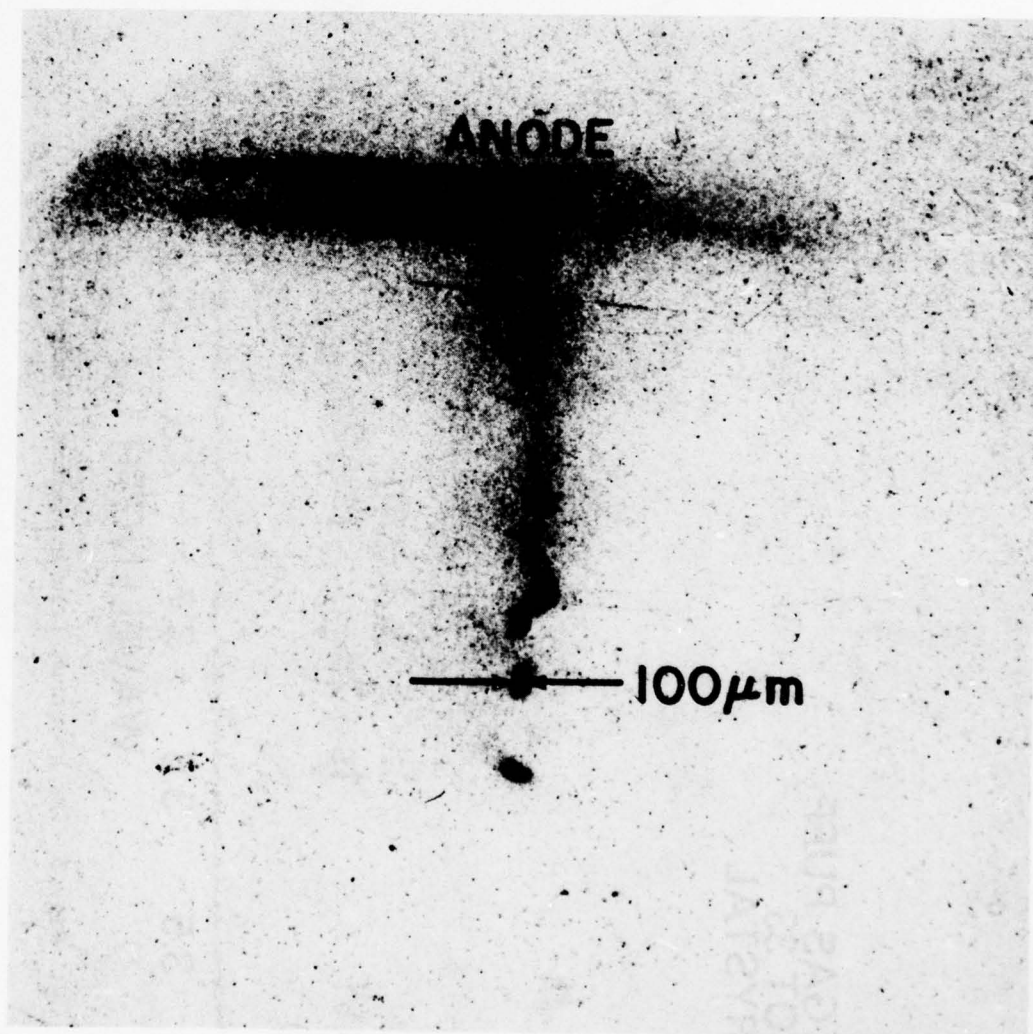
Fig. 4 - Pinhole image of Kr gas-puff plasma.
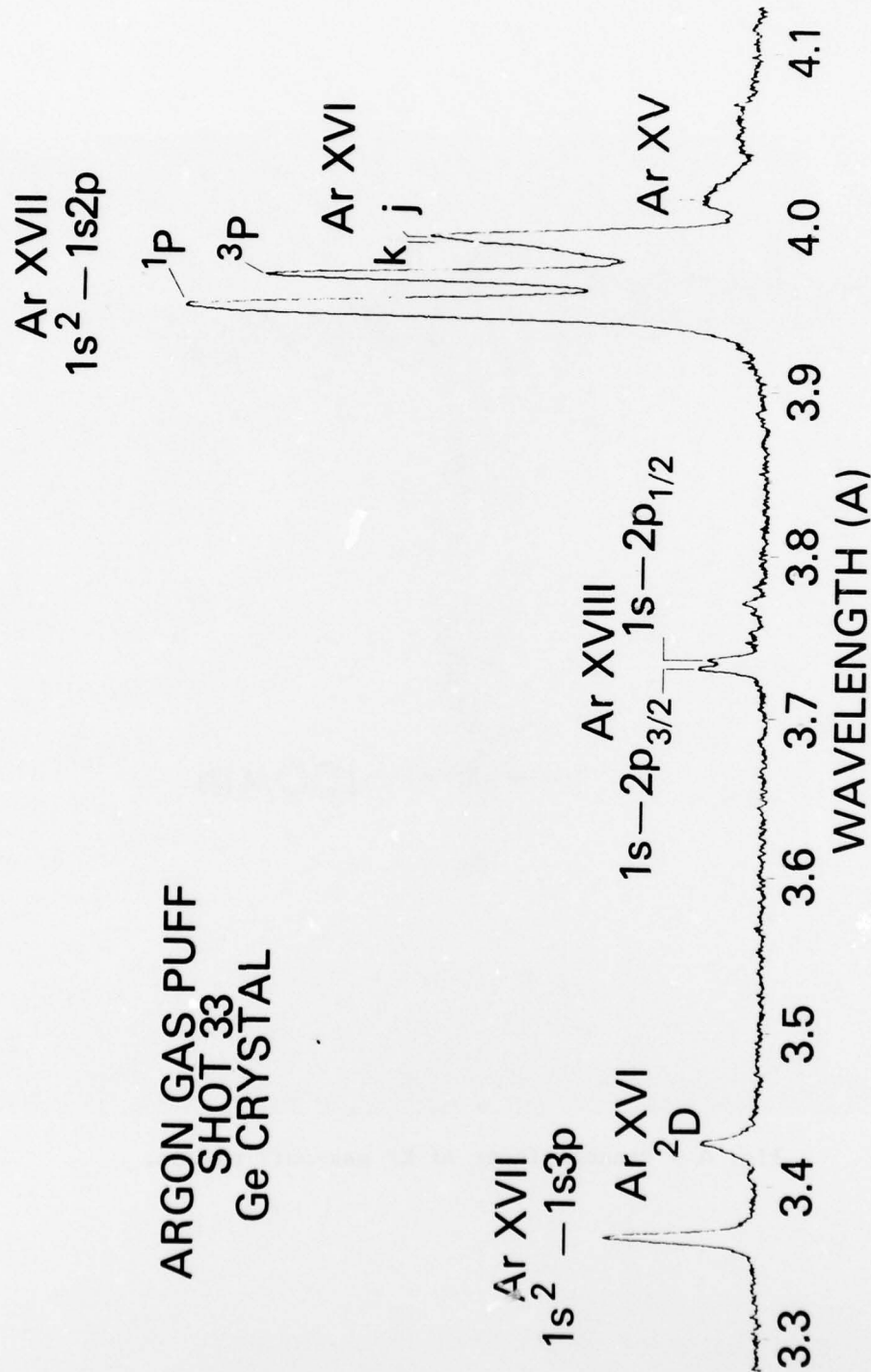
Fig. 5 - Ar spectrum from a pinched-plasma region.
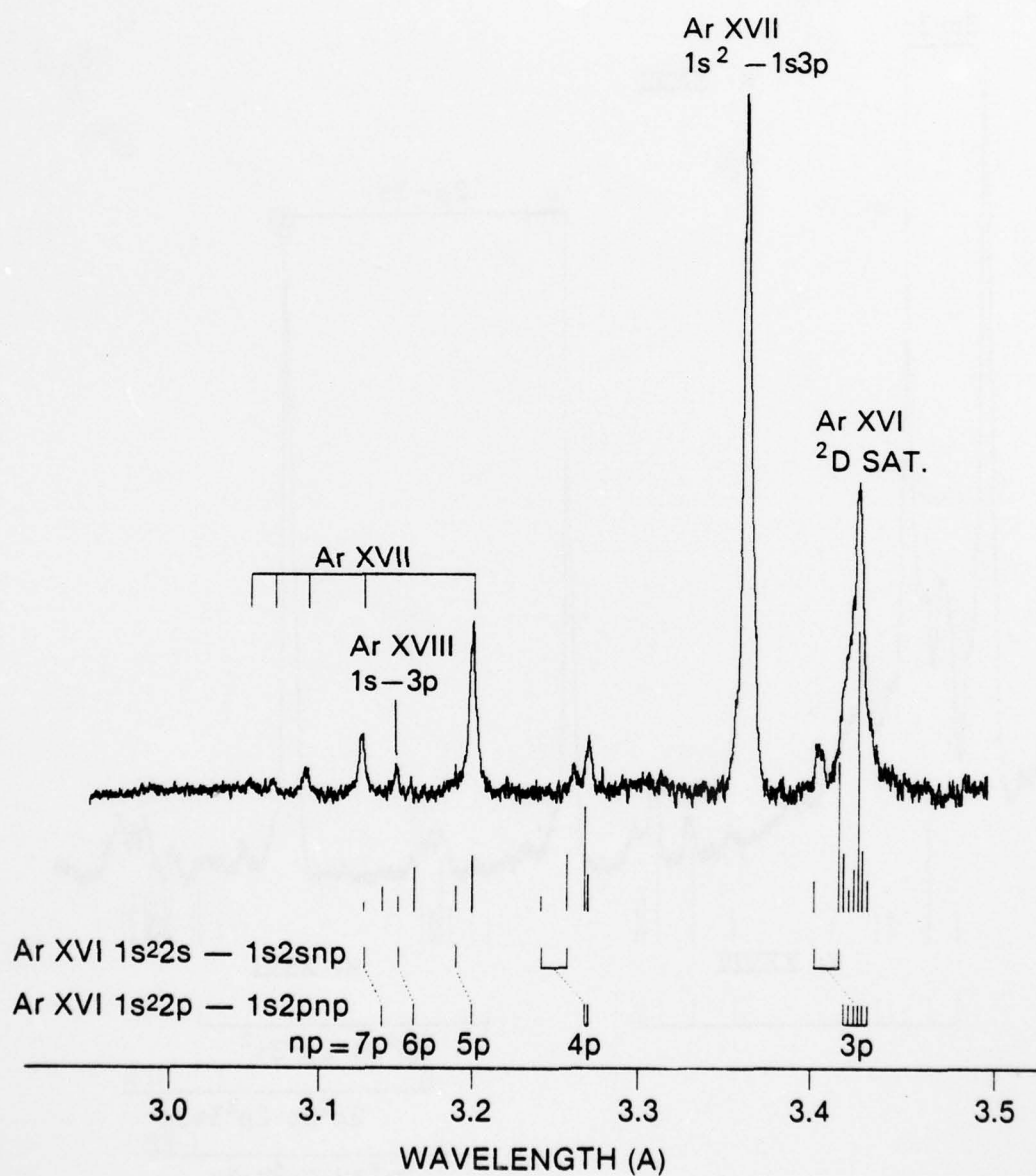
Fig. 6 - Ar spectrum 3-3.5 Å showing the high Rydberg transitions in Ar XVII and Li-like satellite line identifications in Ar XVI.
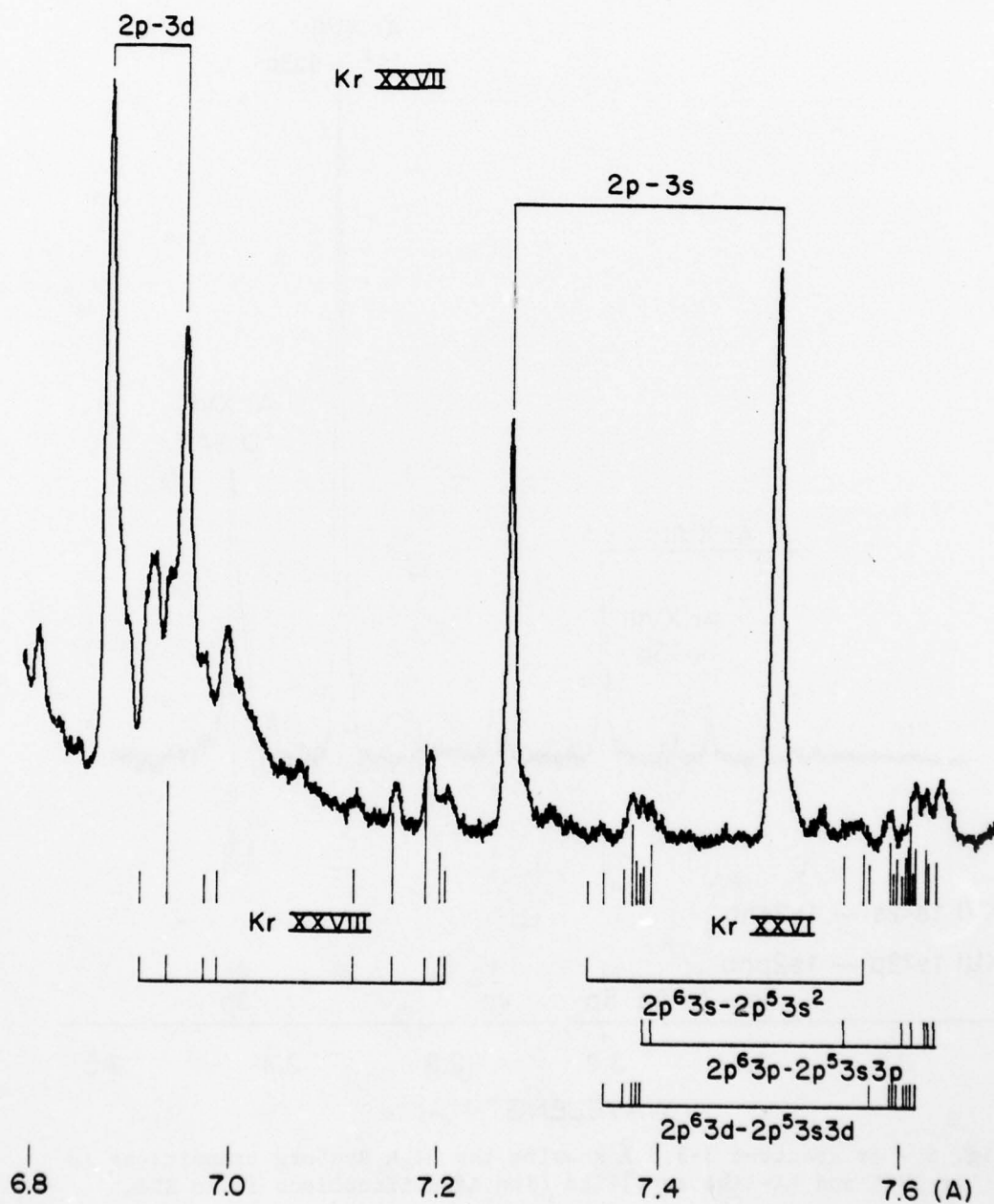
Fig. 7 - Kr spectrum 6.8-7.6 Å showing the 2p-3s
transitions in Kr XXVI thru XXVIII.
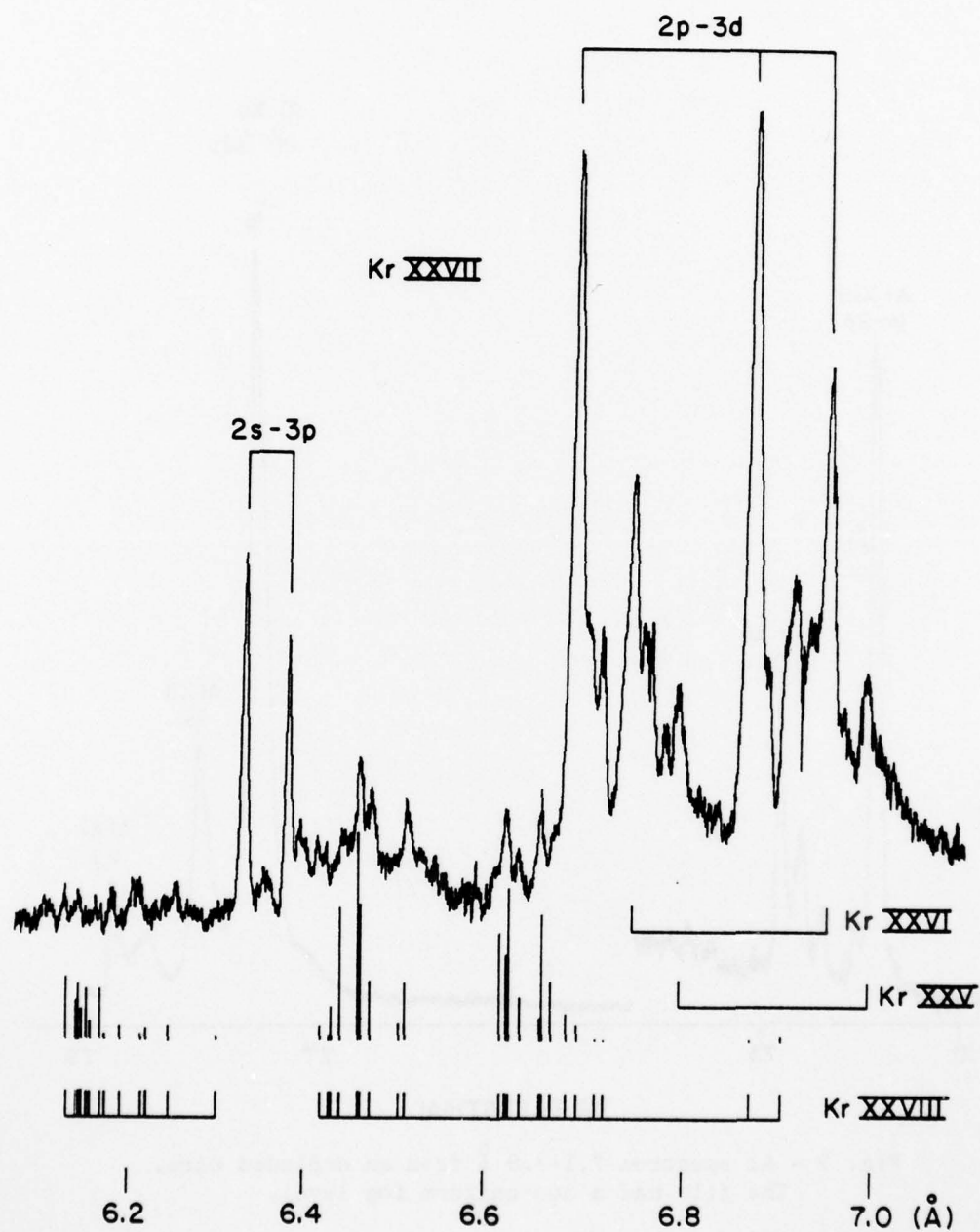
Fig. 8 - Kr spectrum 6-7Å, with identifications for the 2p-3d
and 2s-3p transitions in Kr XXVII and XXVIII.
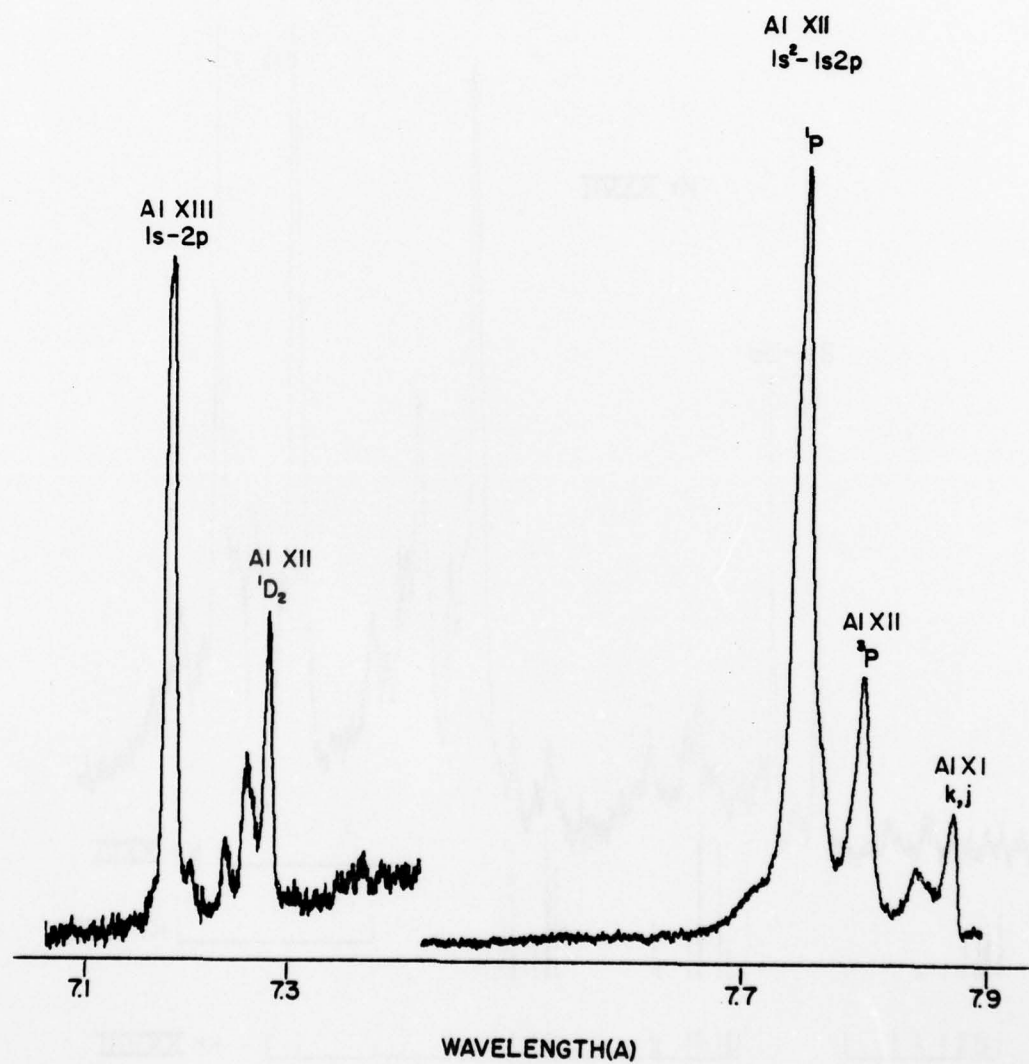
Fig. 9 - Al spectrum 7.1-7.9 Å from an exploded wire.
The film had a non-uniform fog level.
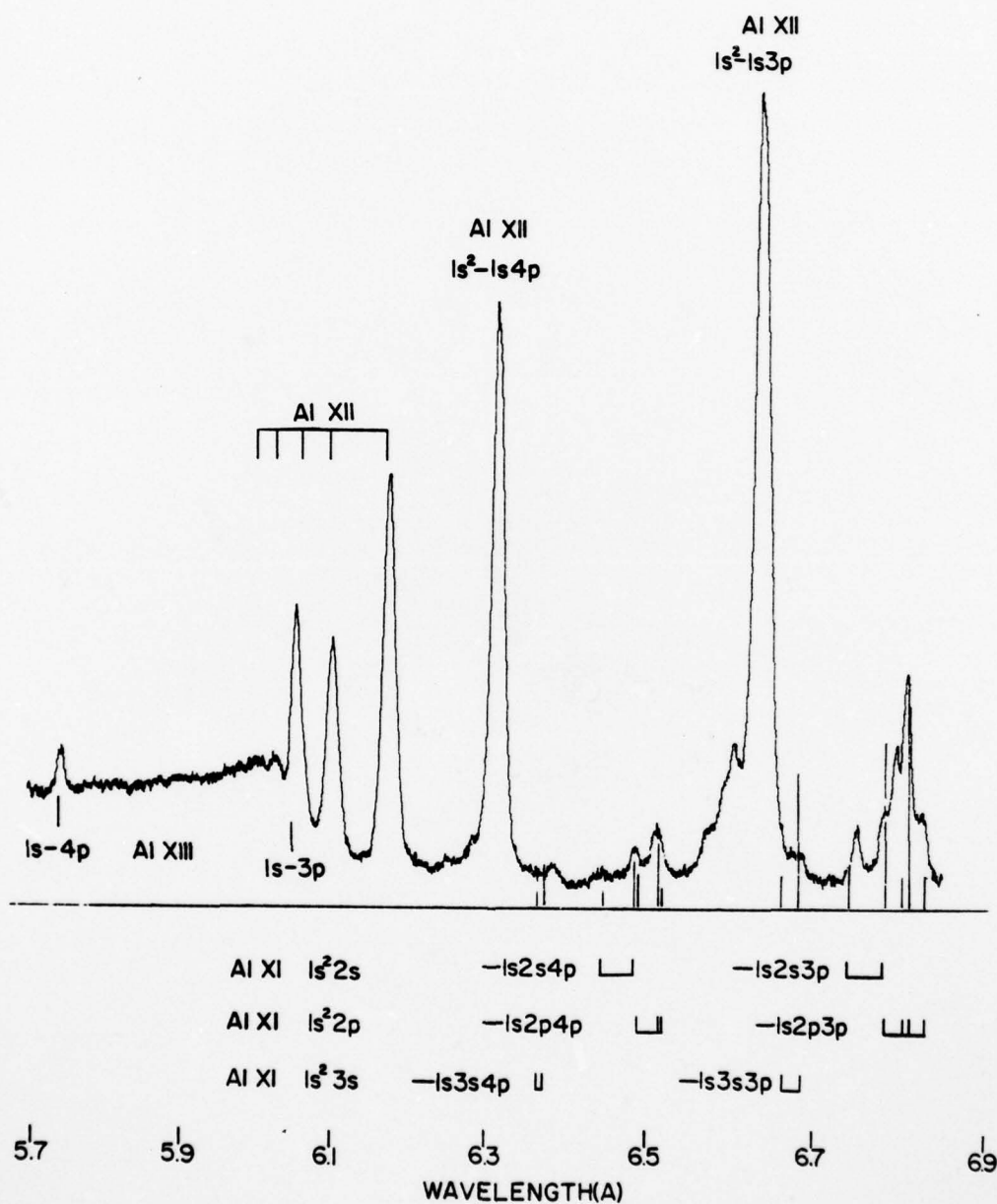
Fig. 10 - Al spectrum 5.7-6.9 Å of the high Rydberg transitions from an exploded wire, with Li-like satellite line identifications in Al XI.

DISTRIBUTION LIST

Assistant to the Secretary of Defense   1 Copy
Atomic Energy   ATSDAE 600208
Washington, D.C. 20301   CNWDI

Attn: Executive Assistant

Defense Documentation Center   (12 copies if open publication,
Cameron Station   otherwise 2 copies)
Alexandria, Virginia 22314   DDC 107200
Attn: DD   CNWDI

Director   1 Copy
Defense Intelligence Agency   DIA 107300
Washington, D.C. 20301   CNWDI
Attn: DT-1B R. Rubenstein

Director   DNA 107050
Defense Nuclear Agency   CNWDI
Washington, D.C. 20305
        Attn: DDST   (1 copy)
        Attn: TITL   (4 copies)
        Attn: RAEV   (1 copy)
        Attn: STVI   (1 copy)

                                                         1 Copy
Commander   DNAFO 400361
Field Command   CNWDI
Defense Nuclear Agency
Kirtland AFB, New Mexico 87115
        Attn: FCPR

Chief   1 Copy
Field Command   LIVDNA 600158
Livermore Division   CNWDI
Department of Defense
P. O. Box 808
Livermore, California 94550
   Attn: FCPRL

Director   1 Copy
Joint Strat TGT Planning Staff   JSTPS 600129
Offutt AFB   CNWDI
Omaha, Nebraska 68113
   Attn: JSAS

Under Secretary of Defense   1 Copy
    For RSCH and ENGRG   USDRE 266200
Department of Defense   CNWDI
Washington, D.C. 20301
    Attn: Strategic and Space Systems (OS)

Deputy Chief of Staff for RSCH DEV and ACQ   1 Copy
Department of the Army   DCSRDA 265950
Washington, D.C. 20301   CNWDI
    Attn: DAMA-CSS-N

Commander   HDL 163050
Harry Diamond Laboratories   CNWDI
Department of the Army
2800 Powder Mill Road
Adelphi, Maryland 20783
        (CNWDI-Inner Envelope: Attn: DELHD-RBH)   (1 copy each)
    Attn: P. Caldwell
    Attn: DELHD-N-NP
    Attn: DELHD-N-RBA J. Rosado
    Attn: DELHD-N-TI (Tech. Lib)

Commander   REDSCI 600593
Redstone Scientific Information Center
U.S. Army R and D Command   3 copies
Redstone Arsenal, Alabama 35809
    Attn: Chief, Documents

Commander   1 copy
U.S. Army Missile R and D Command   AMICOM 040050
Redstone Arsenal, Alabama 35809   CNWDI
    Attn: DRCPM-PE-EA

Commander   USANA 600492
U.S. Army Nuclear and Chemical Agency   CNWDI
7500 Backlick Road
Building 2073   1 Copy
Springfield, Virginia 22150
    Attn: Library

Commander   1 Copy
U.S. Army Test and Evaluation Command   ATFCOM 041750
Aberdeen Proving Ground, Maryland 21005   CNWDI
    Attn: DRSTE-EL

```
Commanding Officer                                        1 COPY
Naval Intelligence Support Center                         NISC 252080
4301 Suitland Road, Bldg. 5
Washington, D.C.  20390
        Attn:  NISC-45


Commander                                                 1 Copy
Naval Weapons Center                                      NWC 403019
China Lake, California  93555                             CNWDI
      Attn: Code 233 (Tech. Lib.)


Office of the Chief of Naval Operations                   1 Copy
Washington, D.C.  20350                                   CNO 264850
        Attn:  R. Blaise                                  CNWDI


Officer in Charge                                         NSWC 250650
White Oak Laboratory                                      CNWDI
Naval Surface Weapons Center
Silver Spring, Maryland  20910
        Attn:  Code R40        (1 copy)
        Attn:  Code F31        (1 copy)


Air Force Weapons Laboratory                              AFWL 013150
Kirtland AFB, New Mexico  87117                           CNWDI
        Attn:  SUL
        Attn:  CA
        Attn:  DYC
        Attn:  DT        (1 copy each)
        Attn:  CA
        Attn:  DYP


Deputy Chief of Staff                                     1 Copy
Research, Development and Accounting                      USAFRD  611421
Department of the Air Force
Washington, D.C.  20330
        Attn:  AFRDQSM

Space and Missile Systems Organization/DY                 1 Copy
Air Force Systems Command                                 SAMSO 611357
Post Office Box 92960                                     CNWDI
Worldway Postal Center
Los Angeles, California  90009
        Attn:  DYS (Technology)
```

Space and Missile Systems Organization/IN   1 Copy
Air Force Systems Command   SAMSO 611392
Post Office Box 92960   CNWDI
Worldway Postal Center
Los Angeles, California   90009
     Attn: IND D. Muskin (Intelligence)

Space and Missile Systems Organization/MN   1 Copy
Air Force Systems Command   NORTON 6C0190
Norton AFB, California 92409   CNWDI
     Attn: MNNH (Minuteman)

Space and Missile Systems Organization/SK   1 Copy
Air Force Systems Command   SAMSO 611397
Post Office Box 92960   CNWDI
Worldway Postal Center
Los Angeles, California 90009
     Attn; SKF P. Stadler (Space Comm. Systems)

AVCO Research and Systems Group   1 Copy
201 Lowell Street   AVNIL 403996
Wilmington, Massachusetts 01887   Fac Clear T CNDWI
     Attn: Library A830   Stor Capability T

BDM Corporation   1 Copy
7915 Jones Branch Drive   BDMVA 404435
McLean, Virginia 22101   Fac Clear T CNWDI
     Attn: Corporate Library)   Stor Capability T

Boeing Company   1 Copy
P. O. Box 3707   BOE 059600
Seattle, Washington 98124   Fac Clear T CNWDI
     Attn: Aerospace Library   Stor Capability T

Dikewood Industries, Inc.   1 Copy
1009 Bradbury Drive, S.E.   DIKEWD 112850
Albuquerque, New Mexico   87106   Fac Clear T CNWDI
     Attn: L. Davis   Stor Capability T

EG and G Washington Analytical Services Center, Inc.   1 Copy
P. O. Box 10218   EGGALB 383316
Albuquerque, New Mexico 87114   Fac Clear T CNWDI
    Attn: Library   Stor Capability S

General Electric Company   1 Copy
Space Division   GESD 149070
Valley Forge Space Center   Fac Clear T CNWDI
P. O. Box 8555   Stor Capability T
Philadelphia, Pa.   19101
    Attn: J. Peden

General Electric Company - Tempo   1 Copy
Center for Advanced Studies   TEMPO 346420
816 State Street   Fac Clear T CNWDI
P. O. Drawer QQ   Stor Capability T
Santa Barbara, California 93102
    Attn: DASIAC

Institute for Defense Analyses   1 Copy
400 Army-Navy Drive   IDA 179350
Arlington, Va. 22202   Fac Clear T CNWDI
    Attn: Classified Library   Stor Capability T

IRT Corporation   1 Copy
P.O. Box 81087   IRT 601410
San Diego, California   92138   Fac Clear T CNWDI
    Attn: R. Mertz   Stor Capability T

JAYCOR   1 Copy
1401 Camino Del Mar   JAYCA 611545
Del Mar, California 92014   Fac Clear T CNWDI
    Attn: E. Wenaas   Stor Capability S

JAYCOR   1 Copy
205 S Whiting Street, Suite 500   JAYVA 611580
Alexandria, Virginia 22304   Fac Clear T CNWDI
    Attn: R. Sullivan   Stor Capability S

KAMAN Sciences Corp.   KN   195000
P. O. Box 7463   FAC Clear T CNWDI
Colorado Springs, Colorado 80933   Stor Capability T
     Attn: J. Hoffman
     Attn: A. Bridges   (1 copy each)
     Attn: D. Bryce
     Attn: W. Ware

Lawrence Livermore Laboratory   LLI   204150
University of California   CNWDI
P. O. Box 808
Livermore, California 94550
     Attn: DOC   CDN for L-545 J. Nickolls   (1 copy each)
     Attn: DOC CDN for L-153
     Attn: DOC CDN for L-47 L. Wouters
     Attn: DOC CDN for Technical Infor. Dept. Lib.

Lockheed Missiles and Space Co., Inc.   LMSC   210120
P. O. Box 504   Fac Clear T CNWDI
Sunnyvale, California 94086   Stor Capability T
     Attn: S. Taimlty

Lockheed Missiles and Space Co., Inc.   1 Copy
3251 Hanover Street   LMSCPA 210110
Palo Alto, California 94304   Fac Clear T CNWDI
     Attn: L. Chase   Stor Capability T

Maxwell Laboratory, Inc.   1 Copy each
9244 Balboa Avenue   MAXLAB 327218
San Diego, California 92123   Fac Clear T CNWDI
     Attn: A. Kolb   Stor Capability S
     Attn: W. Clark

McDonnell Douglas Corp.   1 Copy
5301 Bolsa Avenue   MDCHB 404770
Huntington Beach, California 92647   Fac Clear T CNWDI
     Attn: S. Schneider   Stor Capability T

Mission Research Corp.   1 Copy each
P.O. Drawer 719   MRC 000289
Santa Barbara, California 93102   Fac Clear T CNWDI
    Attn: C. Longmire   Stor Capability S
    Attn: W. Hart

Mission Research Corp.-San Diego   1 Copy
P. O. Box 1209   MRCVLN 400205
La Jolla, California 92038   Fac Clear T CNWDI
    Attn: Victor J. Van Lint   Stor Capability S

Northrop Corporation   1 Copy
Northrop Research and Technology Center   NCPVP
1 Research Park   Fac Clear T CNWDI
Palos Verdes Peninsula, California 90274   Stor Capability S
    Attn: Library

Northrop Corporation   1 Copy
Electronic Division   NOREL. 600302
2301 120th Street   Fac Clear T CNWDI
Hawthorne, California 90250   Stor Capability T
    Attn: V. Damarting

Physics International Company   1 Copy each
2700 Merced Street   PIC 282760
San Leandro, California 94577   Fac Clear S CNWDI
    Attn: P. Spence   Stor Capability S
    Attn: C. Stallings
    Attn: B. Bernstein

R and D Associates   1 Copy each
P. O. Box 9695   RDA 600466
Marina Del Rey, California 90291   Fac Clear T CNWDI
    Attn: W. Graham, Jr.   Stor Capability T
    Attn: C. MacDonald

Sandia Laboratories   1 Copy each
P.O. Box 5800   SANALB 315300
Albuquerque, New Mexico 87115   CNWDI
    Attn: Doc Con For G. Yonas
    Attn: Doc Con For 3141

91

Science Applications, Inc.   SAI 500100
P. O. Box 2351   Fac Clear T CNWDI
La Jolla, California 92038   Stor Capability T
    Attn: J. Beyster

Spire Corporation   SPI 600215
P. O. Box D   Fac Clear T CNWDI
Bedford, Massachusetts 01730   Stor Capability S
    Attn: R. Little

SRI International   SRI 332500
333 Ravenswood Avenue   Fac Clear T CNWDI
Menlo Park, California 94025   Stor Capability T
    Attn: S. Dairiki

Systems, Science and Software, Inc.   Se 388507
P. O. Box 1620   Fac Clear T CNWDI
La Jolla, California 92038   Stor Capability S
    Attn: A. Wilson

Texas Tech University   TXTECU 405703
P. O. Box 5404, North College Station   Fac Clear S
Lubbock, Texas 79417   Stor Capability S
    Attn: T. Simpson

TRW Defense and Space Systems Group   1 Copy
One Space Park   TRWRB 354595
Redondo Beach, California 90278   Fac Clear T CNWDI
    Attn: Technical Information Center   Stor Capability T

Vought Corporation   1 Copy
Michigan Division   Vought 611546
38111 Van Dyke Road   Fac Clear T
Sterling Heights, Maine 48077   Stor Capability T
    Attn: Technical Information Center
           (Formerly LTV Aerospace Corp.)

Director   NRL
Naval Research Laboratory   251950
Washington, D.C. 20375   CNWDI

    Attn: Code 6770 G. Cooperstein
    Attn: Code 6701 J. Brown
    Attn: Code 6707 J. Davis
    Attn: Code 6707 P. Burkhalter   50 copies
    Attn: Code 5565 K. Whitney